NACA

RESEARCH MEMORANDUM

FLIGHT DETERMINATION OF THE DRAG OF CONICAL-SHOCK NOSE

INLETS WITH VARIOUS COWLING SHAPES AND AXIAL

POSITIONS OF THE CENTER BODY AT MACH

NUMBERS FROM 0.8 TO 2.0

By Charles F. Merlet and Leonard W. Putland

Langley Aeronautical Laboratory
Langley Field, Va.

NATIONAL ADVISORY COMMITTEE
FOR AERONAUTICS
WASHINGTON

September 10, 1954
Declassified July 26, 1957

NATIONAL ADVISORY COMMITTEE FOR AERONAUTICS

RESEARCH MEMORANDUM

FLIGHT DETERMINATION OF THE DRAG OF CONICAL-SHOCK NOSE

INLETS WITH VARIOUS COWLING SHAPES AND AXIAL

POSITIONS OF THE CENTER BODY AT MACH

NUMBERS FROM 0.8 TO 2.0

By Charles F. Merlet and Leonard W. Putland

SUMMARY

Free-flight tests were made of conical-shock nose inlet models having cowls of fineness ratio 3 with five different profiles. Three of the profiles were mostly conic, differing primarily in lip shape. The fourth and fifth profiles were parabolic and NACA 1-series, respectively. External drag at an angle of attack of 0° was determined at both supercritical and subcritical flow rates and for three axial locations of the 25° half-angle center body. The Mach number range of the tests was from 0.8 to 2.0, and the Reynolds number based on maximum body diameter varied from 2×10^6 to 7×10^6, respectively.

For the parabolic and conic cowls, changing the axial location of the center body had little effect on the external-drag coefficient for supercritical operation for the range of axial cone positions tested. Changing the external lip angle of the conic cowls from 5° to 17° resulted in only small changes in external drag at maximum flow rates throughout the Mach number range tested. At a Mach number of about 1.1, the minimum external drag appeared independent of profile shape. As the Mach number increased, the drag coefficients of the conic cowls became progressively lower than that of either the parabolic or the 1-series profile.

For Mach numbers greater than 1.5, where theoretical calculations of the additive drag can be made, the measured increase in drag with subcritical spillage was less than the theoretically calculated additive drag. In the Mach number range from 1.1 to 1.4, the external drag of the conical-shock inlet models was, in general, lower than the drag of normal-shock inlet models of similar profiles for a given flow rate, but the increase in drag with subcritical spillage was at least as rapid as the increase in drag due to spillage of the similar normal-shock inlet models.

INTRODUCTION

As part of the inlet research program of the Pilotless Aircraft Research Division of the Langley Aeronautical Laboratory, some of the effects of cowling profile shape on the drag of normal-shock nose inlets were investigated and reported in reference 1. However, because its total-pressure recovery is limited, the normal-shock inlet is of little practical interest at Mach numbers above 1.5. For higher Mach numbers, an external- or internal-compression inlet is capable of developing higher total-pressure recoveries. Therefore, as the next phase of the inlet program, an investigation of conical-shock inlets has been conducted over a range of Mach numbers from 0.8 to 2.0.

The investigation was conducted to determine some of the effects of changes in cowling profile shape and axial cone position on the external drag of some conical-shock inlets, and results are presented for a series of cowls of fineness ratio 3, having inlet cowl areas equal to 24 percent of the maximum body frontal area. The testing technique used was similar to that reported in reference 1. In this case, however, some of the flight tests were augmented by prior ground calibration tests.

SYMBOLS

A area, sq ft

A_{cr} critical area: area at which sonic velocity will be obtained, assuming one-dimensional isentropic process, sq ft

C_D drag coefficient, $\dfrac{D}{\frac{1}{2}\rho_o V_o{}^2 A_f}$

D drag, lb

H total pressure

M Mach number

m/m_o ratio of mass flow of air through the duct to mass flow of air through a free-stream tube of area equal to inlet area defined by lip diameter

p static pressure

R   Reynolds numbers, based on 7.00-inch body diameter

r   radius, in.

V   velocity

x   longitudinal distance, measured from the maximum-diameter
           station, positive downstream, in.

γ ratio of specific heats, 1.40 for air

ρ air density

θ_l cowling position parameter: angle between the inlet axis of
           symmetry and a line joining the tip of the cone to the lip
           of the cowl

Subscripts:

o   free stream

1   inlet minimum annular area station

f   frontal

i   inlet, at lip leading edge

e   exit

int   internal

x   external

MODELS

Conical-shock nose-inlet models having five different cowl shapes
were tested. All cowls were of fineness ratio 3 and had an inlet area
of 24 percent of the body frontal area. The center body employed had
a 25° half-angle cone. The general arrangement of the models, showing
the three axial locations of the cone that were tested, is presented in
figure 1 for a typical profile. The three cone positions, $\theta_l = 46°$,
42.5°, and 39°, corresponded to design Mach numbers of 1.8, 2.0, and 2.3,
respectively. The parabolic afterbody line (table I) and fin configu-
ration (fig. 1) were identical for all models and were the same as for
the models of reference 1. The afterbody, spun of 0.09-inch magnesium
and finished to a smooth, fair contour, formed the after portion of

the duct. The only difference in geometry between models of the same cowl profile was a slight change in afterbody length. The duct exit area was altered as required by cutting off the afterbody at the desired station, thus keeping the pressure drag of the base a negligible quantity by minimizing the area of the base annulus. Flow parallel to the duct center line was insured by the use of convergent inserts with a constant-area section at least 1.2 exit diameters long (fig. 1).

Details of the various cowl shapes tested are shown in figure 2, and coordinates are given in table I. Three of the cowls were formed from truncated cones. The first of these was completely conic, having a half-angle of 4.9°. The external and internal lip angles were 4.9° and 0°, respectively. This will be referred to as the 4.9-conic profile. The second, employing a 4.7° half-angle cone for the major portion of the forebody, was modified in the region of the inlet lips. The initial lip angles were 12° externally and 7° internally. This profile will be designated 12-conic. The third profile employed a 4.4° half-angle cone for most of the forebody with lip angles of 17° externally and 13° internally. This will be designated as the 17-conic profile.

The fourth cowl had the same lip shape as the 17-conic, followed by a short conic section of 7.4° half angle. The remaining portion of the contour had a parabolic-arc profile, defined by a parabola with its vertex at the maximum diameter. This cowl shape will be designated 17-parabolic. The fifth profile tested will be designated the 1-series profile, and was in the notation of reference 2, the NACA 1-49-300. The 4.9-conic and the NACA 1-49-300 cowls were identical to cowls III and II, respectively, of reference 1. The 17-conic employed the same truncated conic forebody as did cowls IV and V of reference 1, but differed in lip shape. The parabolic-arc portion of the 17-parabolic cowl was the same as that of cowl II of reference 1.

For all cowls of the present investigation, the internal lines of the diffuser and the shape of the center body, which were the same for a given profile shape, were designed so that there was no internal contraction for all cone positions tested. To distinguish between models of the same cowl shape, but having different axial locations of the center body, the cowling position parameter θ_l is added to the profile designation. Thus, 17-conic-42.5 will refer to the conic profile having an external lip angle of 17° and a cowling position parameter of 42.5°.

Photographs of the models, showing the various profile shapes, are presented in figure 3. The major physical characteristics have been tabulated and are presented in table II.

TESTS AND TECHNIQUES

All models were propelled to maximum Mach number by a single booster rocket motor equipped with four stabilizing fins. The models were launched at an elevation angle of 60° and followed a zero-lift trajectory at 0° angle of attack. All tests were conducted at the Pilotless Aircraft Research Station at Wallops Island, Va.

Two models, the 17-parabolic-42.5 and the 1-series, used 5-inch HPAG rocket motors as boosters. All the rest used the more powerful 6-inch ABL Deacon rocket motor. The two different rocket motors resulted in different maximum Mach numbers and a slight difference in test Reynolds number, as shown in figure 4.

Total-drag data were obtained during the decelerating portion of the flight, after drag separation of the booster. Computations were based on the CW Doppler radar velocity measurements (corrected for flight-path curvature and winds aloft), the NACA modified SCR 584 radar trajectory measurements, and radiosonde atmospheric measurements. Details of the method of computation are presented in reference 3.

In order to facilitate the construction and testing of a large number of models, all models were flown without telemeter. The internal drag was determined from calculations, in conjunction with a few ground calibration tests made in the preflight jet facility at Wallops Island.

To permit evaluation of internal drag, the models were made so that the flow at the exit would be sonic at supersonic speeds. The fairly large contraction ratio of at least 4 to 1 from near the maximum-diameter station to the exit assured sonic rather than supersonic exit velocities and helped to provide uniform total pressure at the exit. The duct exit was made cylindrical for at least 1.2 exit diameters ahead of the exit to aid in providing uniform static pressure at the exit.

Of the 16 models tested, 10 were designed to operate at supercritical flow rates, while the remainder were designed for subcritical operation. The inlet was considered to be operating supercritically when the normal shock occurred in the diffuser. Conversely, when there was no normal shock in the diffuser, the inlet was considered to be operating subcritically.

The duct exit area of the supercritical models was made larger than the inlet annular area so that the mass flow could be calculated for the Mach number range of the tests. The method of computation is described in the appendix, and the calculated values of m/m_0 and H_e/H_0 are compared with measured values in figure 5 for a supercritical model.

The subcritical models had exit areas smaller than the inlet
annular areas. For these models, the variations of exit total-pressure
recovery and mass-flow ratio with Mach number, necessary for the evalu-
ation of internal drag, were determined from ground tests in the manner
described in the appendix.

At $M_0 \leqq 1.0$, when the exit was no longer sonic, the internal drag
was assumed to be constant at the value calculated for $M_0 = 1.0$. Data
presented in reference 1 and other unpublished data obtained from
normal-shock inlet models indicate this assumption to be valid with
$\Delta C_{D_i} = 0.003$.

The external drag is defined herein as the sum of the dragwise
components of the aerodynamic pressure and viscous forces acting on the
external surfaces of the model (exclusive of the center body) plus the
dragwise component of the aerodynamic forces acting on the external
contour of the entering streamline. The external drag was obtained by
subtracting the internal drag from the total drag determined from the
Doppler radar. The data are believed to be accurate within the following
limits:

m/m_0 . . . . ± 0.02
C_{D_x} . . . . ± 0.01
M . . . . ± 0.01

RESULTS AND DISCUSSION

Basic Data

The curves of external drag coefficient as a function of Mach number
for all configurations tested are presented in figure 6. The mass-flow
ratio curve associated with each drag curve is also given. The measured
maximum mass-flow ratios are shown for those models tested in the pre-
flight jet. The data for the subcritical model 12-conic-46 are shown
as a faired curve below a Mach number of 1.45 because excessive scatter
of approximately twice the previously noted estimated accuracy occurred
in the total-drag values in this Mach number range.

For those profiles where data are presented for both supercritical
and subcritical operation of the inlet, the only difference in model
geometry is the afterbody length. Data presented in reference 1 for the
indentical afterbody shape indicated that this difference in body length
resulted in a maximum difference in external drag coefficient of about
0.003 for Mach numbers up to 1.5. It is therefore believed that the
effect of afterbody length on the external drag coefficients presented
herein is within the accuracy of the data at all Mach numbers.

Effect of Cone Position

Three profile shapes, 12-conic, 17-conic, and 17-parabolic, were tested with alternate axial locations of the center body while maintaining supercritical flow rates. As shown in figure 7, the effect of varying θ_l on external drag was the same for all three profiles. There was little or no difference in external drag as a result of varying the axial location of the cone. Similar results are presented in reference 4 for a curved cowl having an inlet area equal to 43 percent of the maximum frontal area.

Comparison of Profile Shapes

The external drag coefficients for various profiles are compared for $\theta_l = 46^\circ$ in figure 8(a) and for $\theta_l \approx 42.5^\circ$ in figure 8(b). All data are presented for supercritical flow rates. Because the center body of the 12-conic-42.5 (fig. 8(b)) was inadvertently made undersize, the mass-flow ratio for this model is somewhat higher than for the other models at transonic speeds. At $M \approx 1.1$, the effect of profile shape on the drag was small. As the Mach number increased, the conic profiles had the least drag while the 1-series had the most. The drag coefficient of the parabolic-profile model became somewhat higher than that of the conic, being about 0.03 higher at $M = 1.9$ (fig. 8(a)). The effect of altering the lip and forebody angles of the conic profiles appears to be small throughout the Mach number range. These trends are consistent with the results presented in reference 1 for normal-shock inlets.

Effect of Mass-Flow Ratio

Figure 9 presents the external drag coefficient as a function of mass-flow ratio for the various profiles at two Mach numbers. Points are shown for both supercritical and subcritical operation. The two Mach numbers selected are typical of two supersonic regions of flow. At $M > 1.5$, the flow aft of the conical shock is completely supersonic, and theoretical estimates of the additive drag may be made relatively easily. The data for $M = 1.8$ are presented as typical of this region and are compared with the theoretical slope of the additive drag coefficient determined by the method of reference 5. These slopes were then arbitrarily faired through the experimentally determined external drag coefficient at maximum flow. The increase in drag due to subcritical spillage was consistently less than the theoretical estimates of additive drag for all profiles tested. At supercritical flow rates, however, only the 17-parabolic profile showed less increase in drag than the theoretical estimates. Significant decreases in drag were achieved at a given mass-flow ratio by altering the cone position to reduce the flow rate supercritically rather than operating the inlet subcritically.

For $M < 1.5$, theoretical estimates of the additive drag are more difficult to make accurately and, in the Mach number region from 1.1 to 1.4, the data have been compared with the data of reference 1 for normal-shock inlets having similar profiles. The results of this comparison are illustrated by the data for $M = 1.3$. The 4.9-conic and the 1-series profiles are compared with normal-shock inlets having the same external lines. The 12-conic and 17-conic profiles are compared with the beveled-lip conic profile of reference 1, which was formed from a 4.4° half-angle truncated cone modified to have an initial lip angle of 9.8°. The 17-parabolic profile is compared with the parabolic-arc profile of reference 1 which had an initial lip angle of 9.8°.

With the exception of the 1-series profile, the conical-shock models had lower drag than the comparable normal-shock inlets at any given flow rate for the range of mass-flow ratios tested. At the same flow rate, the 1-series conical-shock inlet had essentially the same drag at all Mach numbers tested as did the NACA 1-49-300 normal-shock inlet at the flow rates investigated (fig. 9(e)). For the 17-conic (fig. 9(c)) and the 17-parabolic (fig. 9(d)) profiles, varying θ_l allowed as much as 15-percent reduction in supercritical flow rate without significantly affecting the drag. Decreasing the flow rate subcritically caused the drag of the conical-shock inlets to rise at least as rapidly as did the drag of the comparable normal-shock inlet at reduced flow rates.

CONCLUSIONS

Conical-shock inlet models, having cowls of fineness ratio 3, were tested over a range of Mach numbers from 0.8 to 2.0, both at supercritical and at subcritical flow rates. Five cowling profiles were tested. Three of these were mostly conic, differing primarily in lip shape. The fourth and fifth profiles were parabolic and NACA 1-series, respectively. The results of these tests and comparison with previously published data indicate the following conclusions:

1. For the parabolic and conic cowls, changing the axial location of the center bodies had little effect on the external drag coefficient for supercritical operation for the range of axial cone positions tested.

2. Changing the external lip angle of the conic cowls from 5° to 17° had little effect on the external drag at maximum flow rates throughout the Mach number range tested.

3. At $M \approx 1.1$, the minimum external drag appeared independent of profile shape. As Mach number increased, the drag coefficients of the conic cowls became progressively lower than either the parabolic or the 1-series profile.

4. For M > 1.5, where theoretical additive drag calculations can
be made, the measured increase in drag with subcritical spillage was
less than the theoretically calculated values of additive drag.

5. The external drag of the conical-shock inlet models with conic
or parabolic cowls was lower than the drag of normal-shock inlet models
of similar profile for a given flow rate for Mach numbers from 1.1 to
1.4, when comparative data were available.

6. In the Mach number range from 1.1 to 1.4, the increase in drag
of the conical-shock inlet models as flow rate was decreased subcritically
was at least as rapid as the increase in drag due to spillage of normal-
shock inlet models of similar profile.

Langley Aeronautical Laboratory,
        National Advisory Committee for Aeronautics,
                Langley Field, Va., July 9, 1954.

APPENDIX

The external drag was defined in the usual manner as the dragwise component of the aerodynamic pressure and viscous forces acting on the external surface of the body plus the dragwise component of the aerodynamic pressure forces acting on the external contour of the entering streamline. The external drag was obtained by subtracting the internal drag from the total drag obtained from the CW Doppler radar and SCR 584 tracking radar measurements obtained in the manner indicated in reference 3. The internal drag was obtained by applying the momentum equation between the free stream ahead of the model and the duct exit:

$$D_{int} = \gamma p_o M_o^2 A_o - \gamma p_e M_e^2 A_e - (p_e - p_o) A_e \qquad (A1)$$

For all models, the exit was designed so that $M_e = 1.0$ for $M_o > 1.0$. The procedure used to determine the area of the entering free-stream tube A_o and the duct exit static pressure p_e differed for supercritical and subcritical models, and is indicated below. For $M_o < 1.0$, when the exit was no longer sonic, C_{D_i} was assumed constant at the value obtained at $M_o = 1.0$, for both supercritical and subcritical models.

Supercritical Operation of the Inlet

For $M_o > 1.4$, the variation of A_o, and hence of m/m_o, with M_o can be calculated by means of conical flow theory for a given inlet geometry. The curves presented in reference 6, obtained in this manner, were used in the present paper.

For $M_o < 1.4$, the following equation was used to calculate A_o, where the Mach number at the inlet is assumed to be sonic:

$$A_o = \frac{(H_i/H_o)}{(A_{cr}/A)_o} A_1 \qquad (A2)$$

A_1, the inlet minimum annular area, was calculated by averaging the areas taken perpendicular to the inlet internal lip and perpendicular to the surface of the center body. Two values of inlet total-pressure recovery H_i/H_o were used in equation (A2), a value of 1.0 and a value equal to normal-shock recovery, resulting in two significantly different values of A_o for $M_o > 1.3$. A smooth curve, faired from $M_o = 1.0$

between the points obtained in the above indicated manner, joined the curve obtained from conical-flow theory at $M > 1.4$. For $M_O < 1.0$, A_O was calculated using an inlet recovery of 1.0 in equation (A2), thus completing the curve of A_O as a function of free-stream Mach number for the range of the tests. An average total pressure at the exit can now be calculated from equation (A2) rewritten in terms of the sonic exit:

$$H_e = \left(\frac{A_{cr}}{A}\right)_O \frac{A_O}{A_e} H_O \tag{A3}$$

and thus, for $M_e = 1.0$,

$$p_e = 0.528 H_e \tag{A4}$$

Subcritical Operation of the Inlet

The subcritical values of A_O were obtained from calibration tests made in the preflight jet of the Pilotless Aircraft Research Station at Wallops Island, Va. (ref. 7). The variation of exit total-pressure recovery with mass-flow ratio was measured for three models, 4.9-conic-42.5, 12-conic-42.5, and 17-conic-42.5, at each of four Mach numbers, 1.17, 1.42, 1.62, and 2.06. From the curves of exit total-pressure recovery as a function of mass-flow ratio which were obtained, the values of H_e/H_O and A_O which satisfy equation (A3) for the exit area used with the subcritical flight model were determined at each of the four test Mach numbers. Curves of A_O and H_e/H_O as a function of M_O were then faired, allowing determination of $C_{D_{int}}$ by equation (A1).

REFERENCES

1. Sears, R. I., Merlet, C. F., and Putland, L. W.: Flight Determination
   of Drag of Normal-Shock Nose Inlets With Various Cowling Profiles at
   Mach Numbers From 0.9 to 1.5. NACA RM L53I25a, 1953.

2. Baals, Donald D., Smith, Norman F., and Wright, John B.: The
   Development and Application of High-Critical-Speed Nose Inlets.
   NACA Rep. 920, 1948 (Supersedes NACA ACR L5F30a).

3. Wallskog, Harvey A., and Hart, Roger G.: Investigation of the Drag
   of Blunt-Nosed Bodies of Revolution in Free Flight at Mach Numbers
   From 0.6 to 2.3. NACA RM L53D14a, 1953.

4. Gorton, Gerald C.: Investigation of Translating-Spike Supersonic
   Inlet as Means of Mass-Flow Control at Mach Numbers of 1.5, 1.8,
   and 2.0. NACA RM E53G10, 1953.

5. Sibulkin, Merwin: Theoretical and Experimental Investigation of
   Additive Drag. NACA RM E51B13, 1951.

6. Fraenkel, L. E.: Some Curves for Use in Calculations of the Perfor-
   mance of Conical Centrebody Intakes at Supersonic Speeds and at
   Full Mass Flow. Tech. Note No. Aero. 2135, British R.A.E., Dec. 1951.

7. Faget, Maxime A., Watson, Raymond S., and Bartlett, Walter A., Jr.:
   Free-Jet Tests of a 6.5-Inch-Diameter Ram-Jet Engine at Mach Numbers
   of 1.81 and 2.00. NACA RM L50L06, 1951.

TABLE I.- EXTERNAL COORDINATES OF CONICAL-SHOCK MODELS

[From maximum diameter]

Afterbody
(all models)

x	r
0	3.50
5.60	3.45
10.27	3.34
15.87	3.14
21.47	2.84
24.27	2.65
30.80	2.15
35.70	1.68
42.70	.90

Forebody

x	r
4.9-conic	
-21.00	1.71
-10.00	2.65
0	3.50
12-conic	
-21.00	1.715
-20.75	1.760
-20.50	1.810
-20.25	1.850
0	3.500
17-conic	
-21.00	1.715
-20.75	1.791
-20.50	1.868
-20.25	1.913
-20.00	1.945
-19.75	1.978
0	3.500

Forebody

x	r
17-parabolic	
-21.00	1.715
-20.75	1.791
-20.50	1.868
-20.25	1.913
-20.00	1.945
-19.75	1.978
-16.00	2.464
-15.00	2.589
-10.00	3.095
-5.00	3.399
0	3.500
1-series	
-21.00	1.71
-20.79	1.90
-20.37	2.04
-19.95	2.15
-17.85	2.52
-14.70	2.87
-10.50	3.19
-6.30	3.39
0	3.50

TABLE II.- PHYSICAL CHARACTERISTICS OF MODELS

Designation	θ_l, deg	Forebody profile	Lip angle, deg		Inlet diam., in.	Exit diam., in.	
			External	Internal		Super-critical	Sub-critical
4.9-conic	42.4	Conic, 4.9° half-angle	4.9	0	3.42	3.106	2.765
12-conic	46 42.4	Conic, 4.7° half-angle	12	7	3.43	3.235 3.106	2.869 -----
17-conic	46 42.5 39	Conic, 4.4° half-angle	17	13	3.43	3.235 3.106 2.970	2.869 2.765 -----
17-parabolic	46 42.5 39	Parabolic	17	13	3.43	3.235 3.112 2.970	2.869 2.765 -----
1-series	42.3	NACA 1-49-300	90	0	3.42	3.112	-----
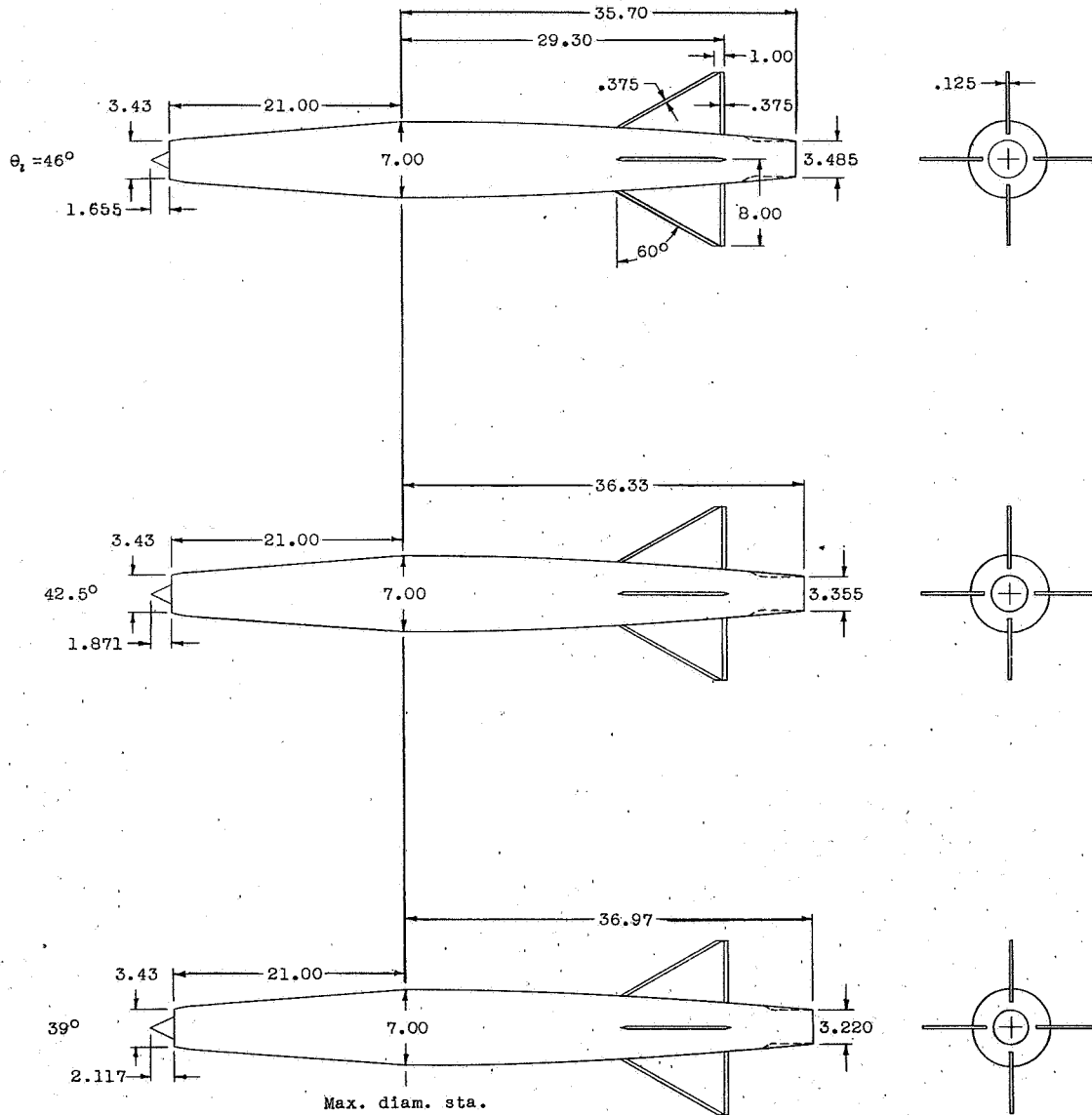
Figure 1.- General arrangement of models.   17-conic.   All dimensions are in inches.
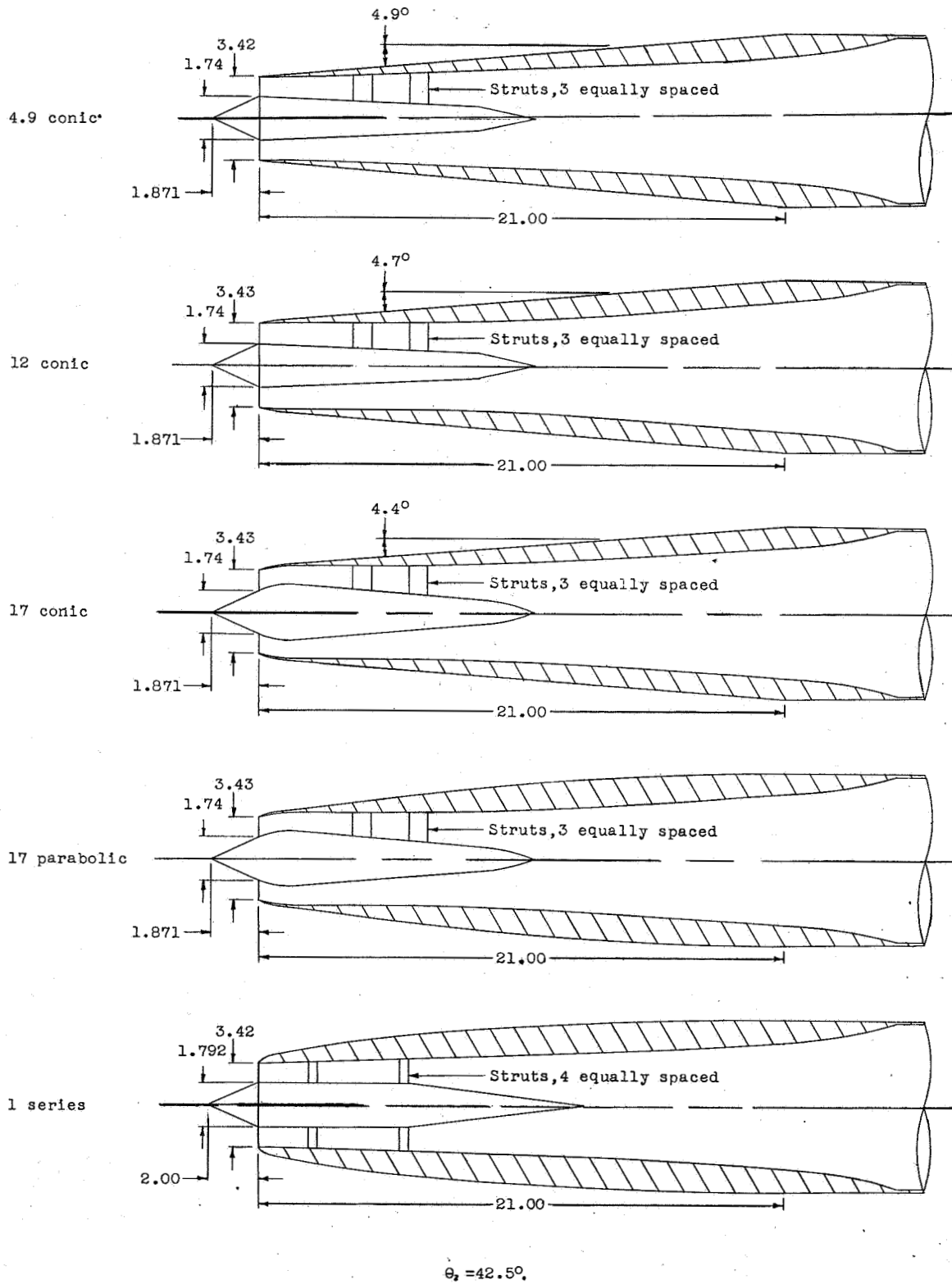
Figure 2.- Details of cowl shapes. $\theta_l = 42.5^{\circ}$. All dimensions are in inches.
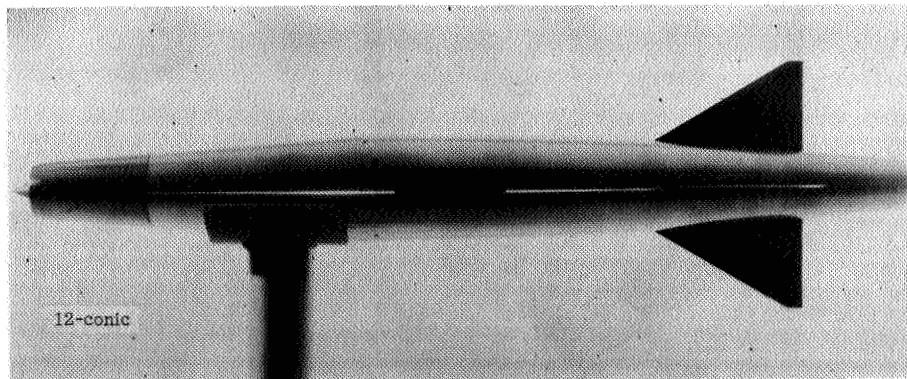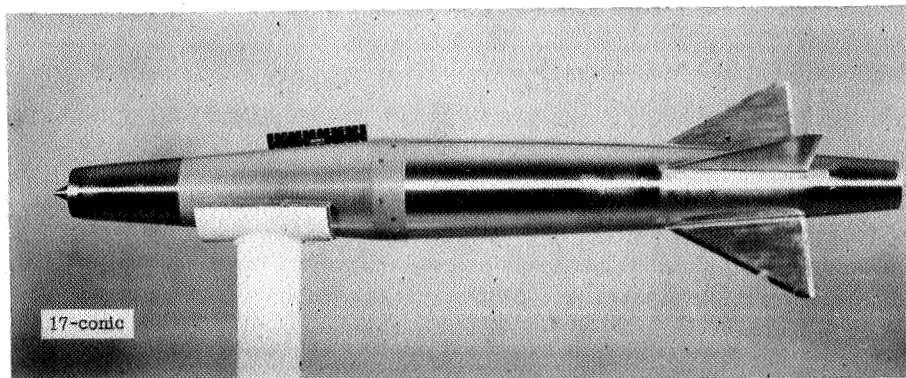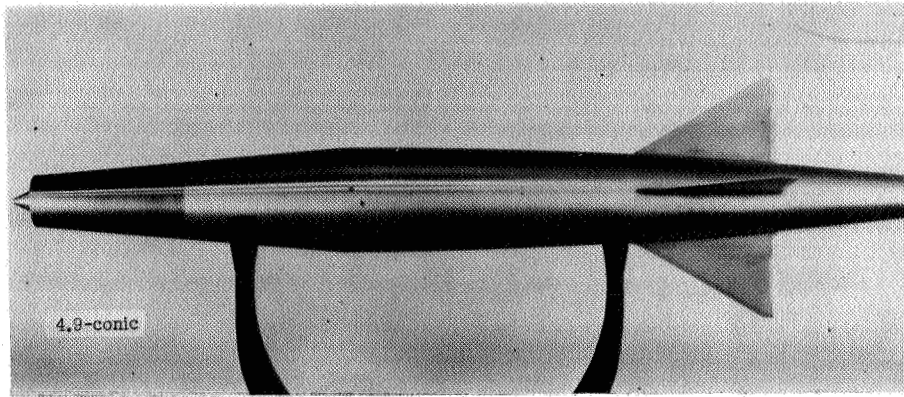
(a) General views.   L-84928

Figure 3.- Photographs of models.

17-parabolic

1-series
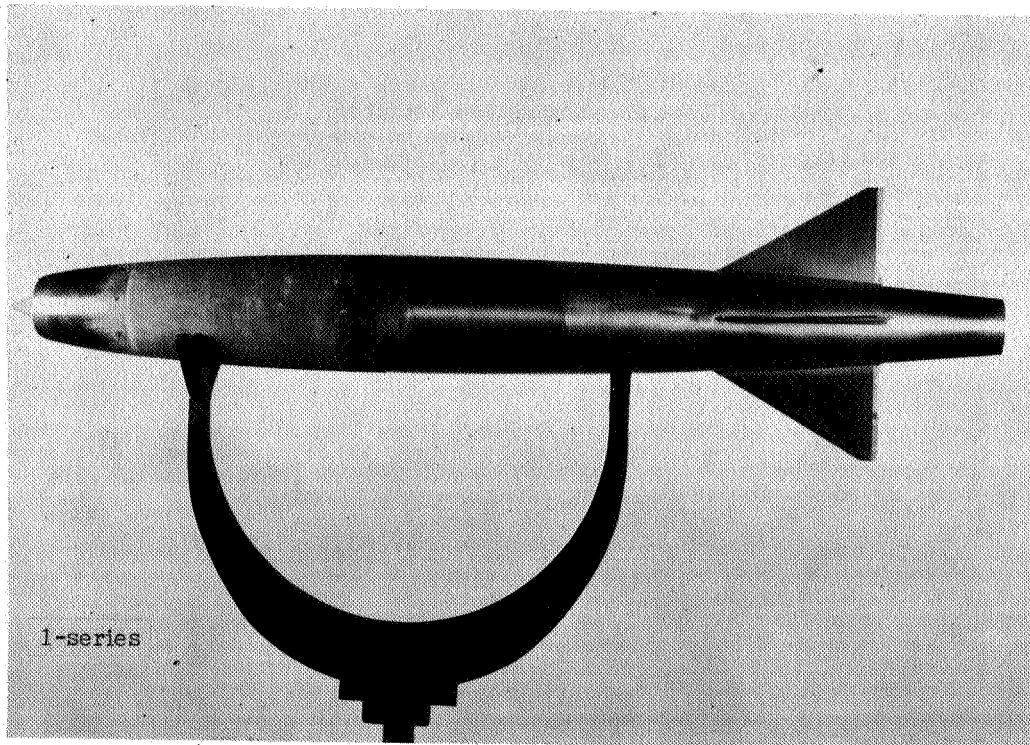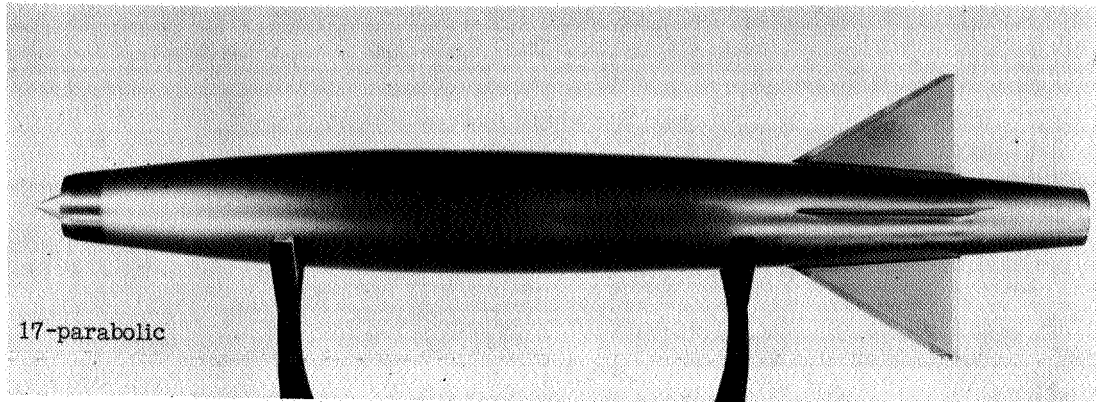
(a) Concluded.   L-84929

Figure 3.- Continued.
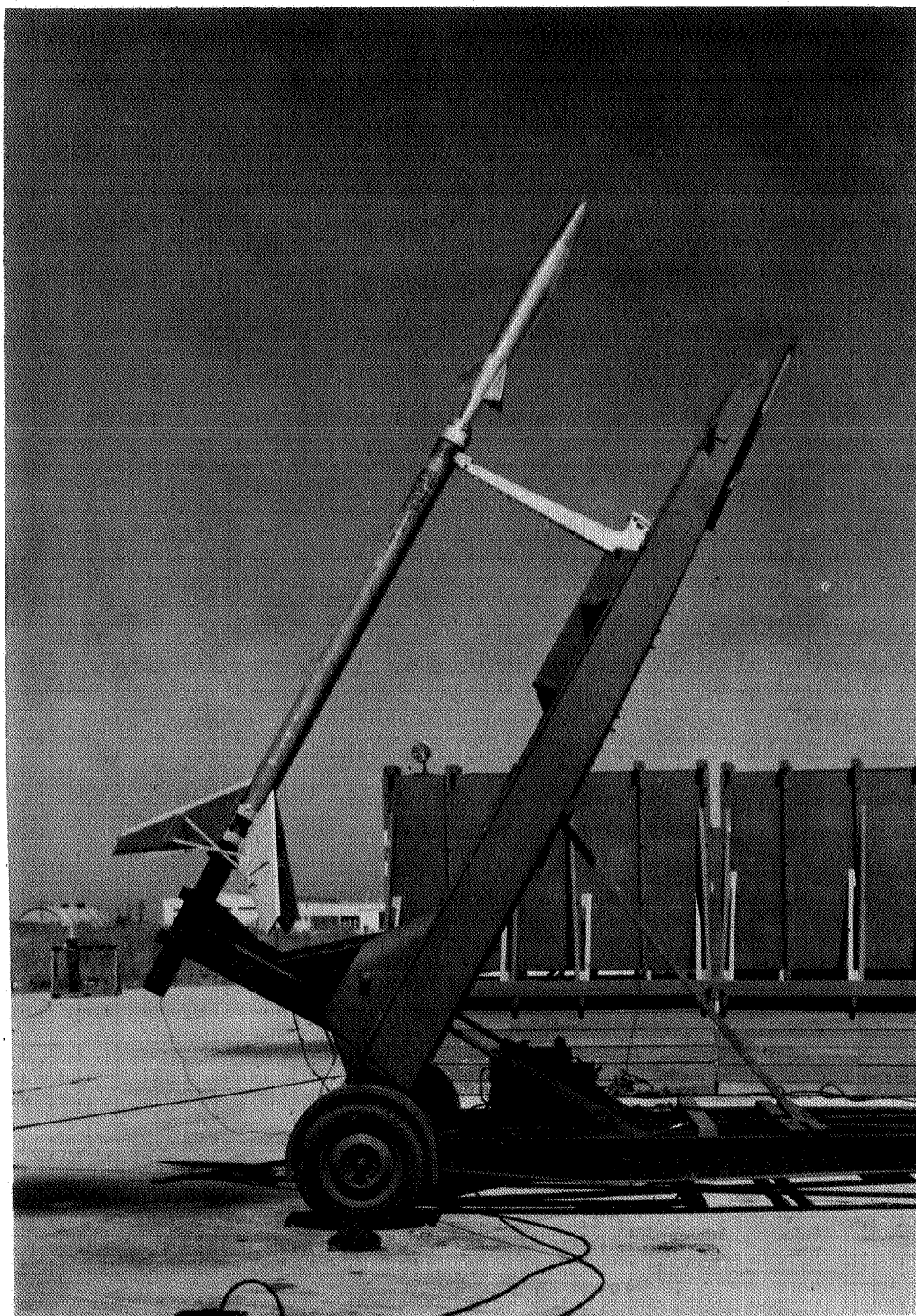
(b) Typical model-booster arrangement.   L-81624.1

Figure 3.- Concluded.
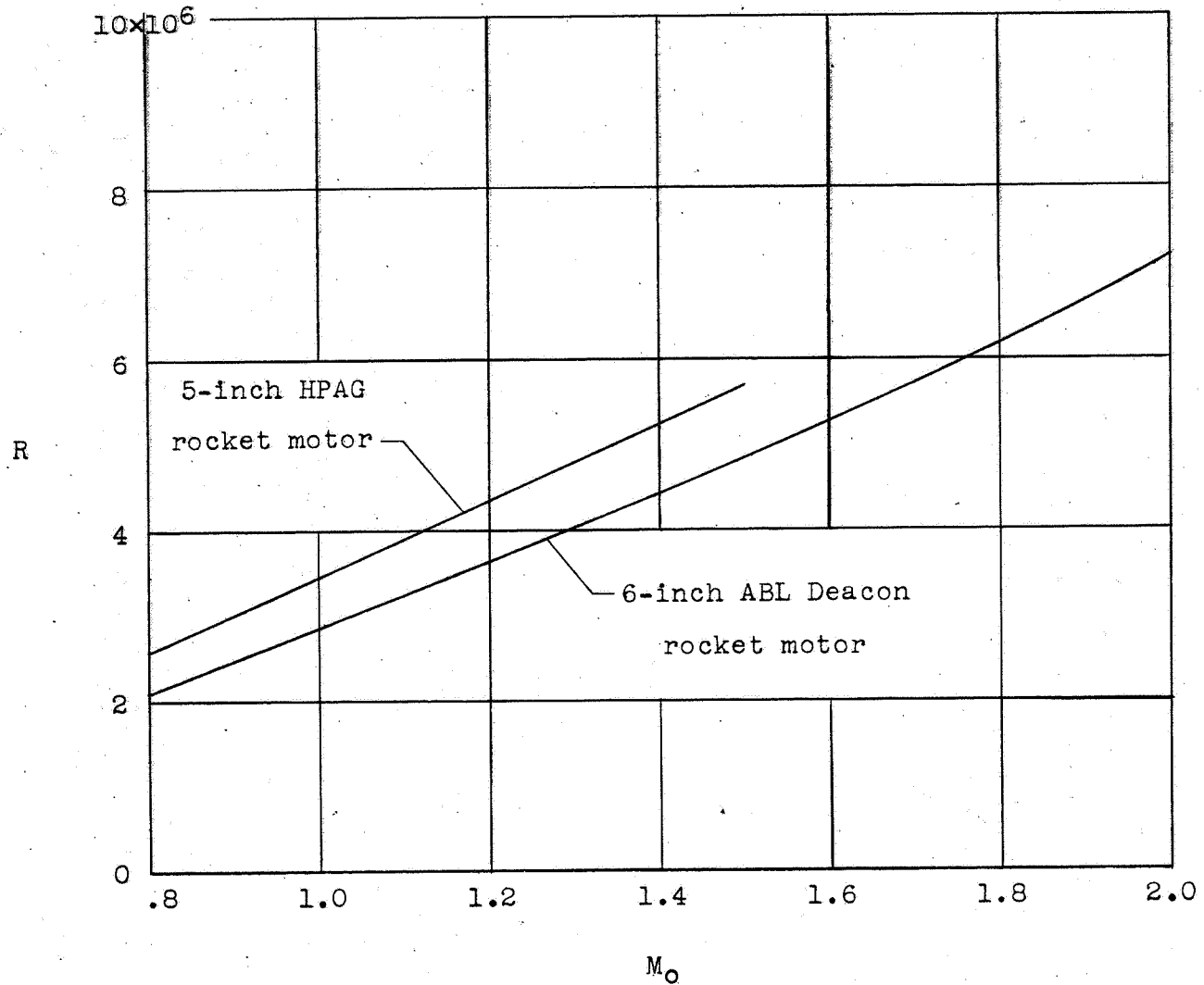
Figure 4.- Reynolds number, based on 7.00-inch body diameter, as a function of Mach number for the two booster rocket motors employed.

H_e/H_o

m/m_o

$\dfrac{H_e/H_o}{\text{and}}$
m/m_o

Mass-flow ratio
△   Inlet total-pressure recovery of 1.0
▽   Inlet total-pressure recovery
         equal to normal shock
▷   Conical-flow theory
◇   Measured values

Total-pressure recovery
   O   Measured values

M_o
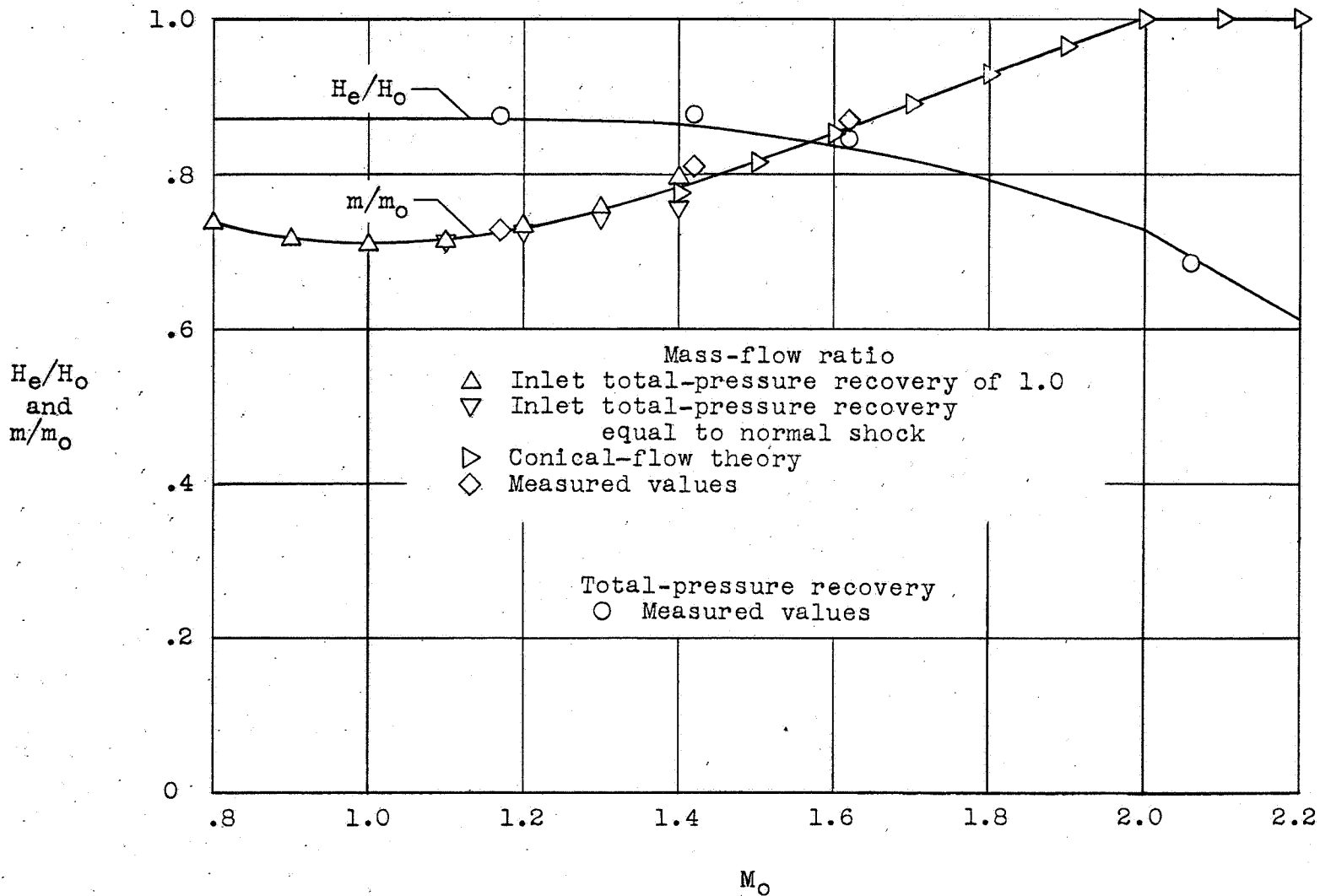
Figure 5.- Measured and theoretical variations of mass-flow ratio and
   exit total-pressure recovery with Mach number for a typical model
   with supercritical flow.
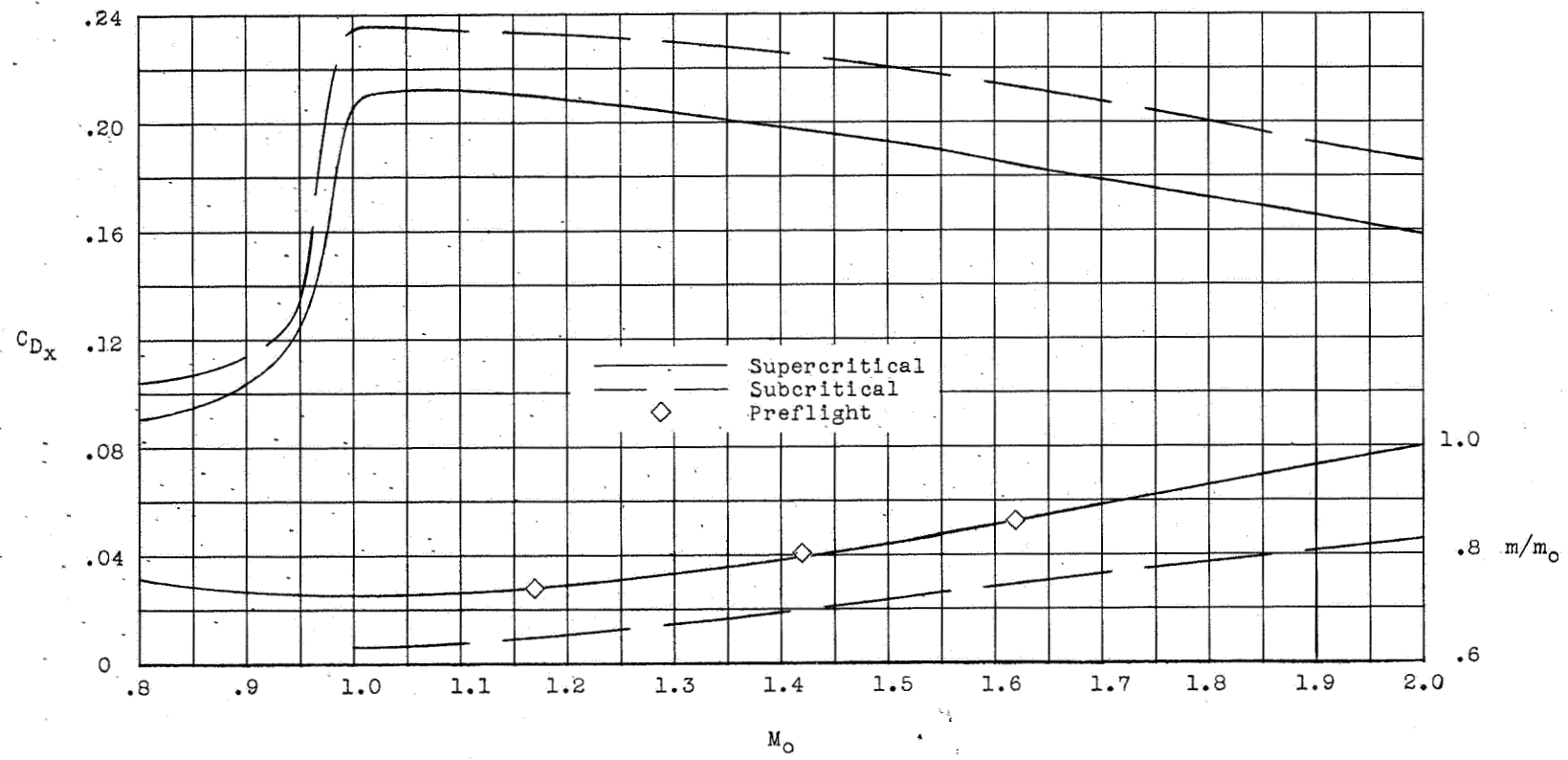
(a) 4.9-conic-42.5.

Figure 6.- Variation of external drag and mass-flow ratio with Mach number
for the models with various profiles and cowling position parameters.
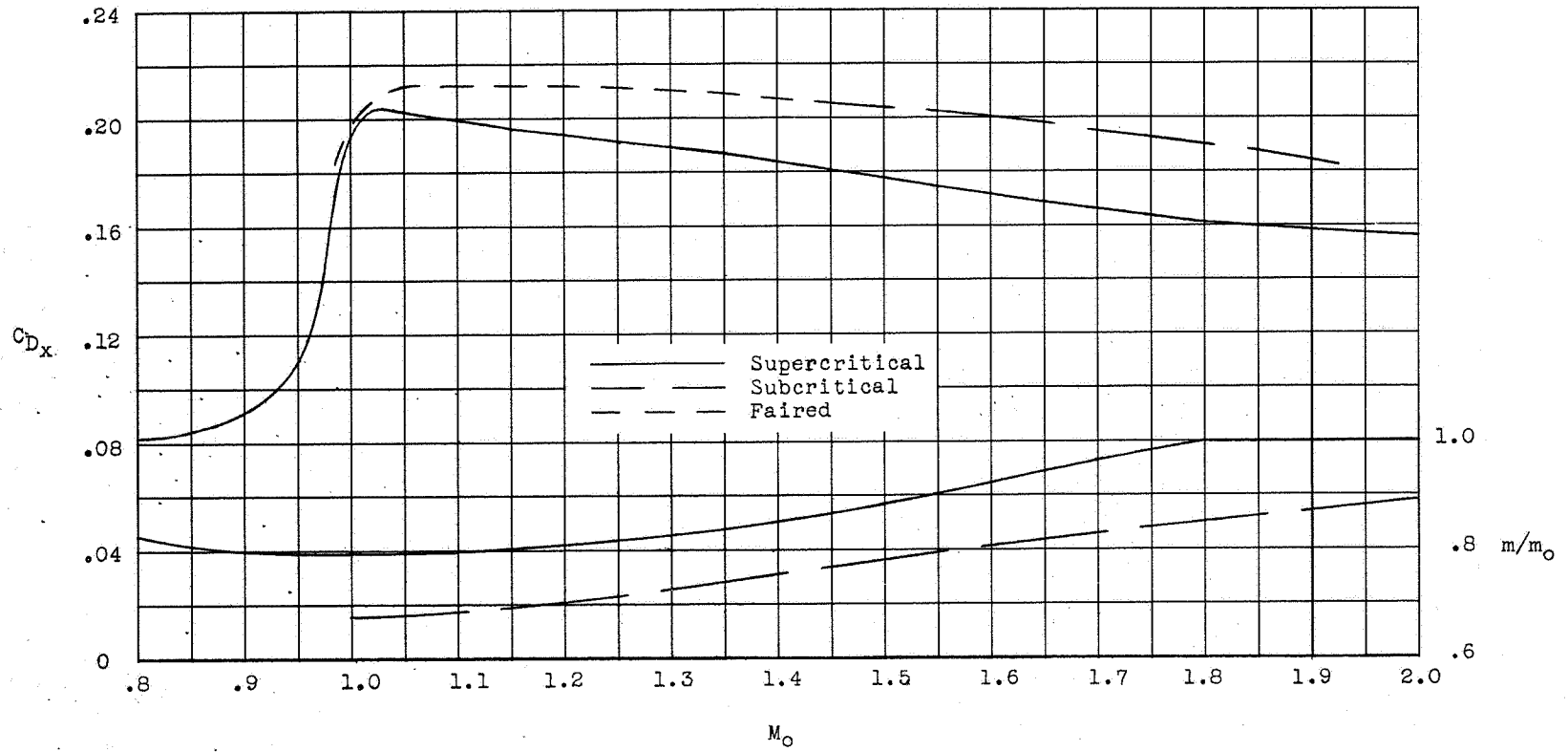
(b) 12-conic-46.

Figure 6.- Continued.
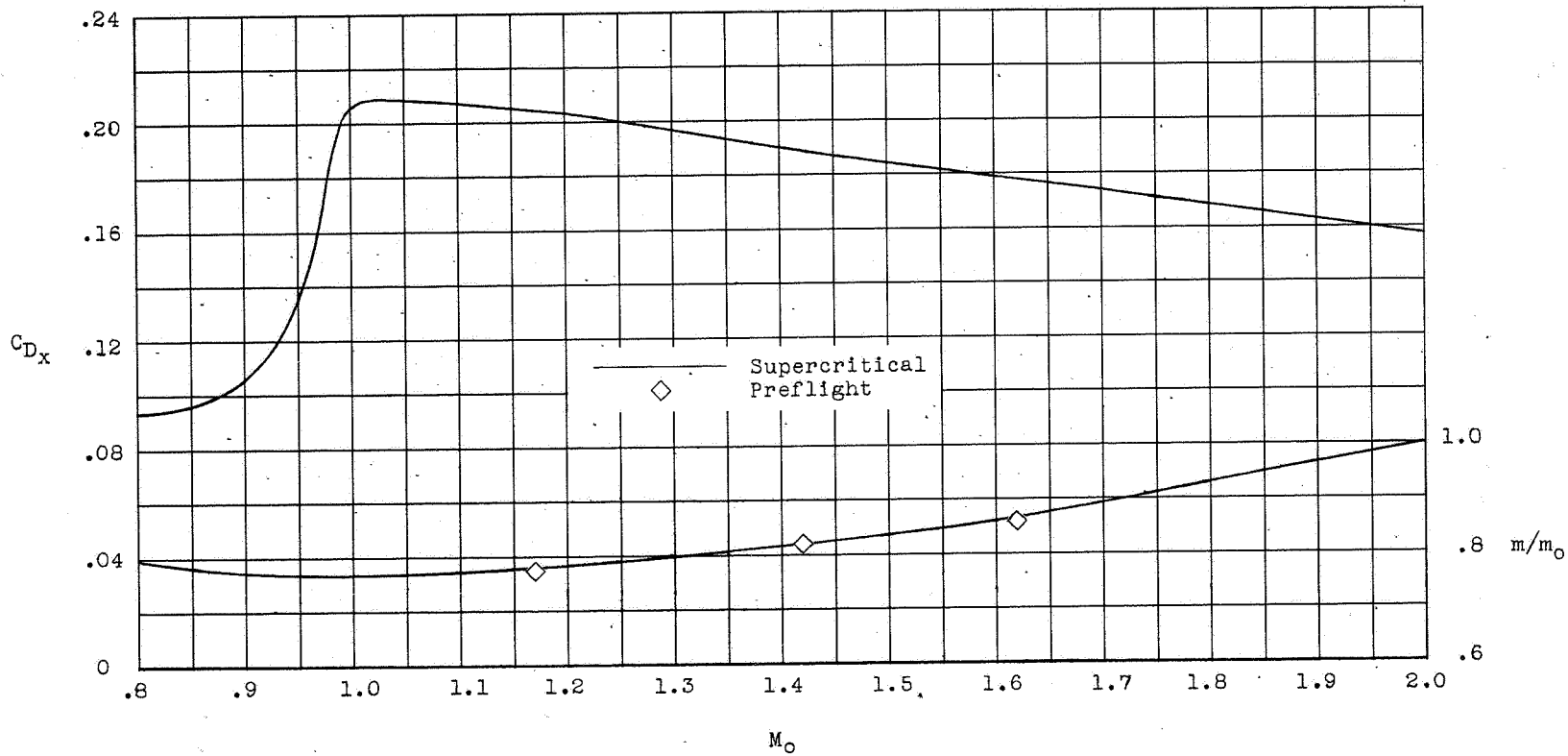
(c) 12-conic-42.5.

Figure 6.- Continued.
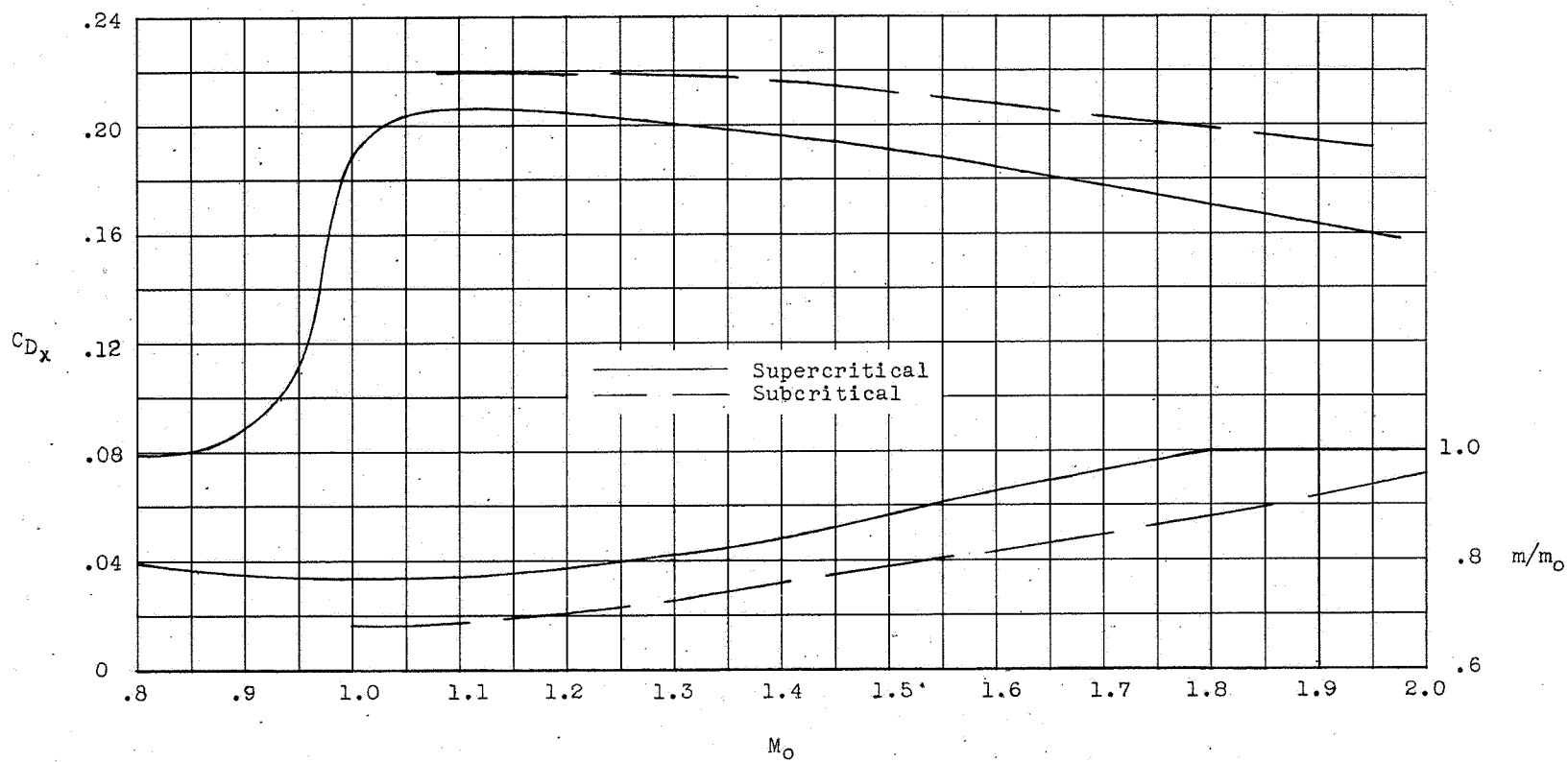
(d) 17-conic-46.

Figure 6.- Continued.
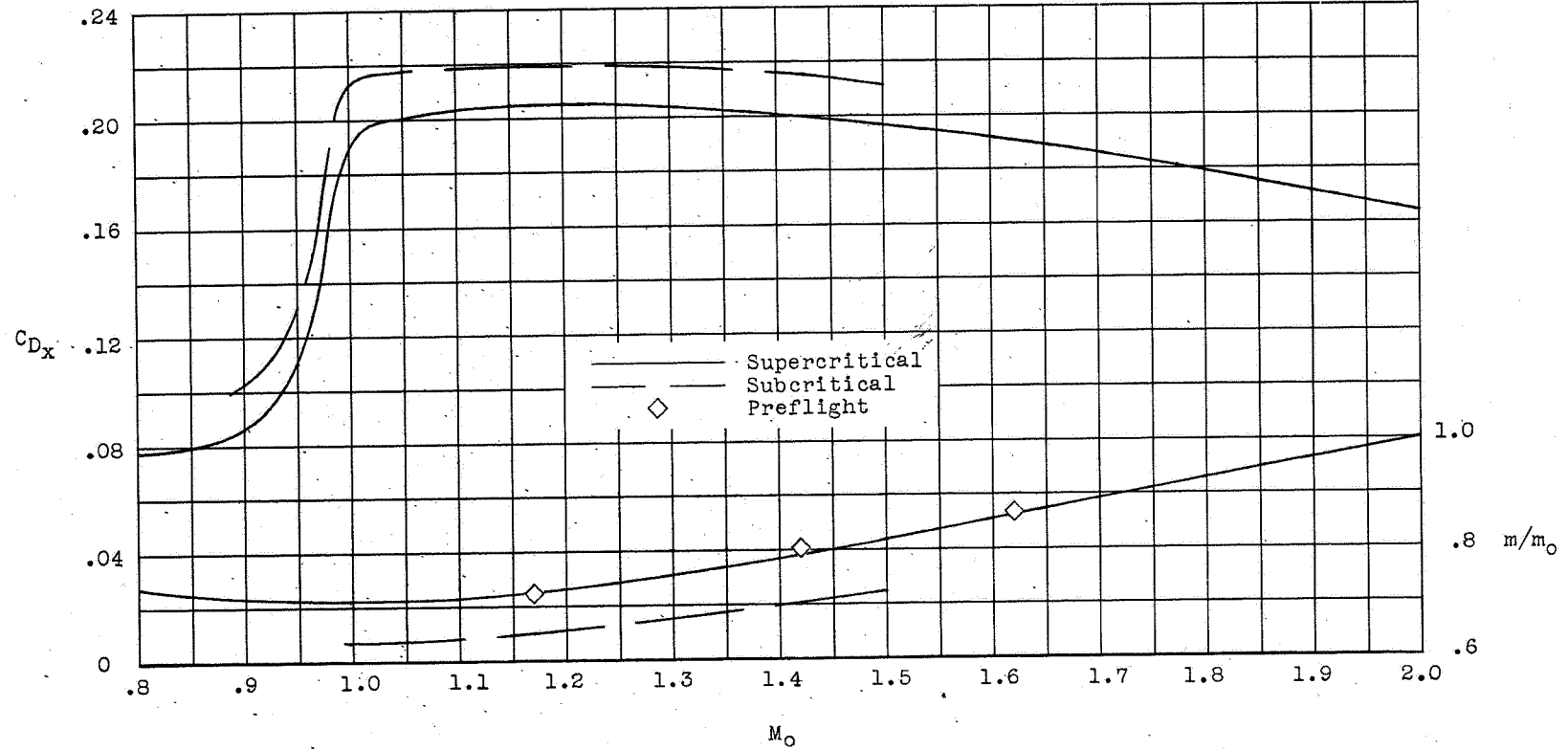
(e) 17-conic-42.5.

Figure 6.- Continued.
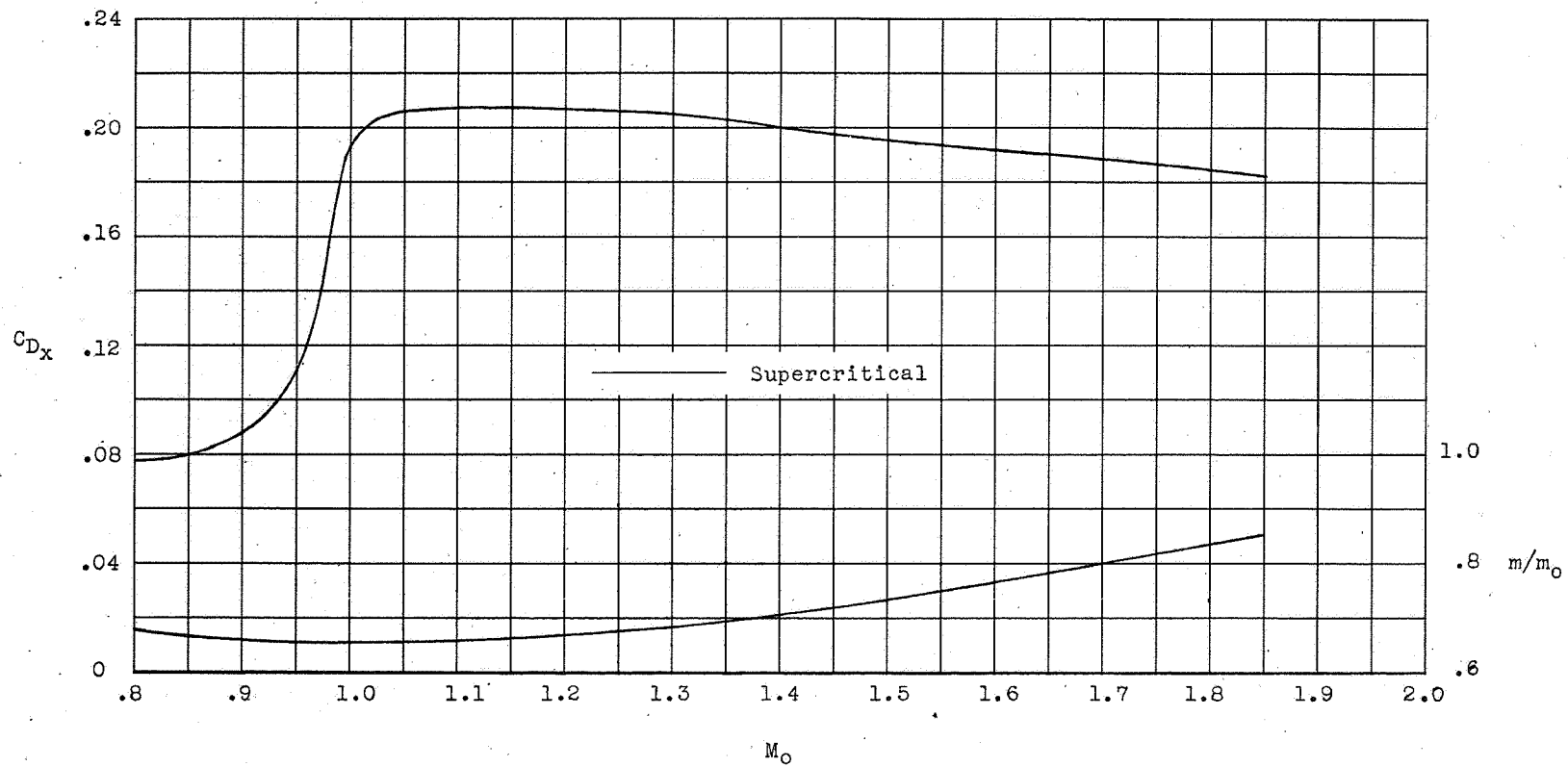
(f) 17-conic-39.

Figure 6.- Continued.
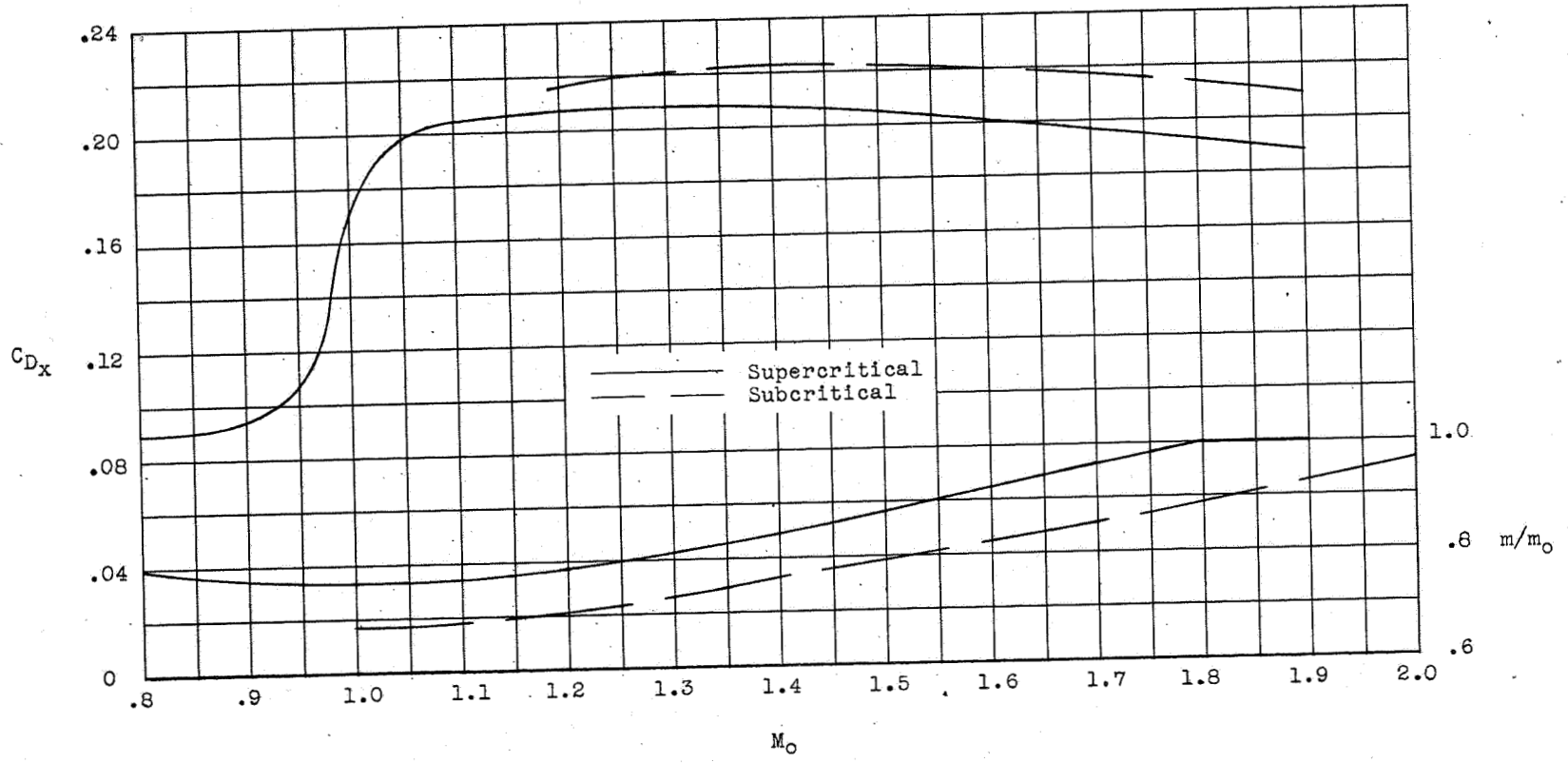
(g) 17-parabolic-46.

Figure 6.- Continued.
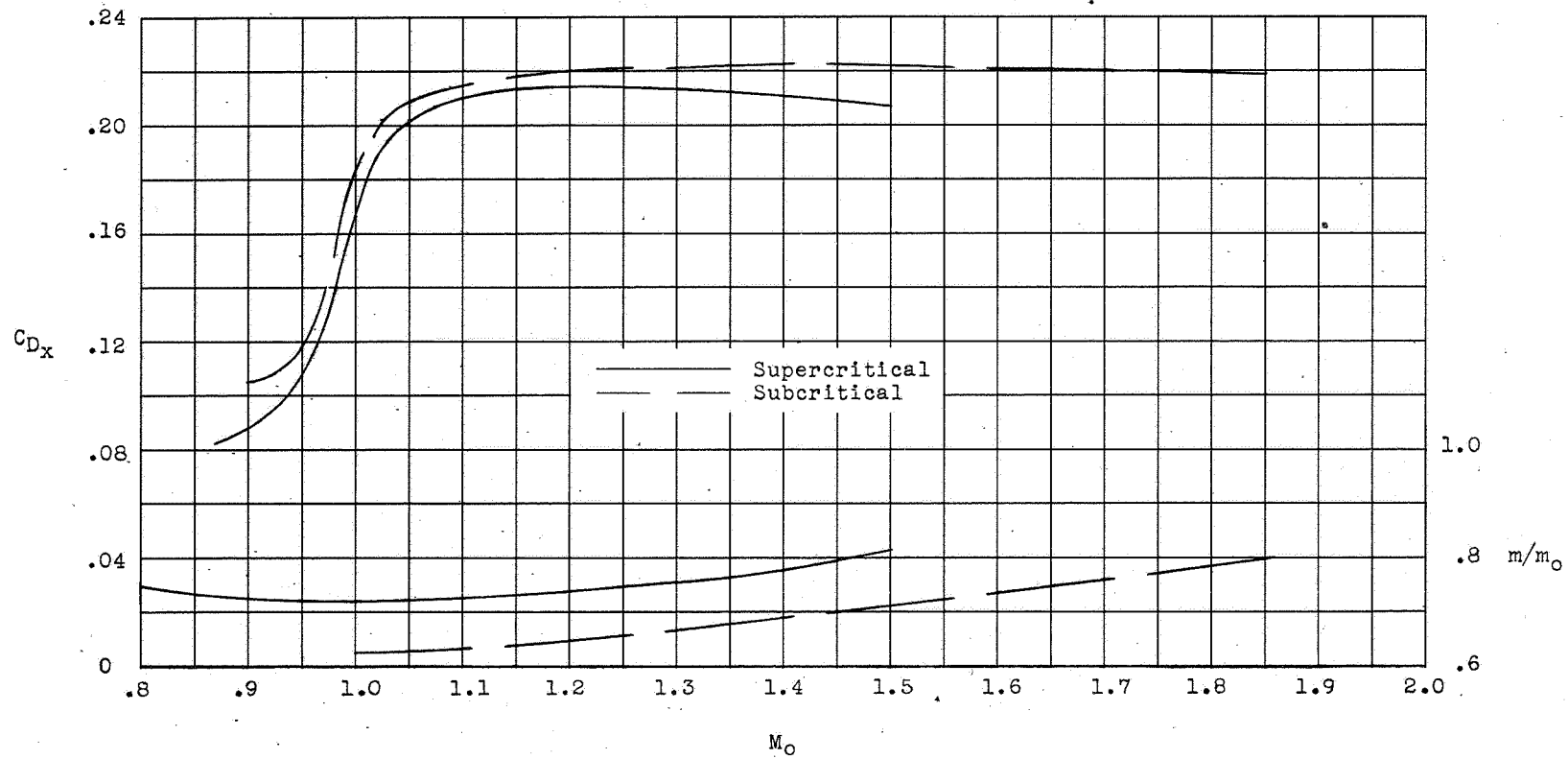
(h) 17-parabolic-42.5.

Figure 6.- Continued.
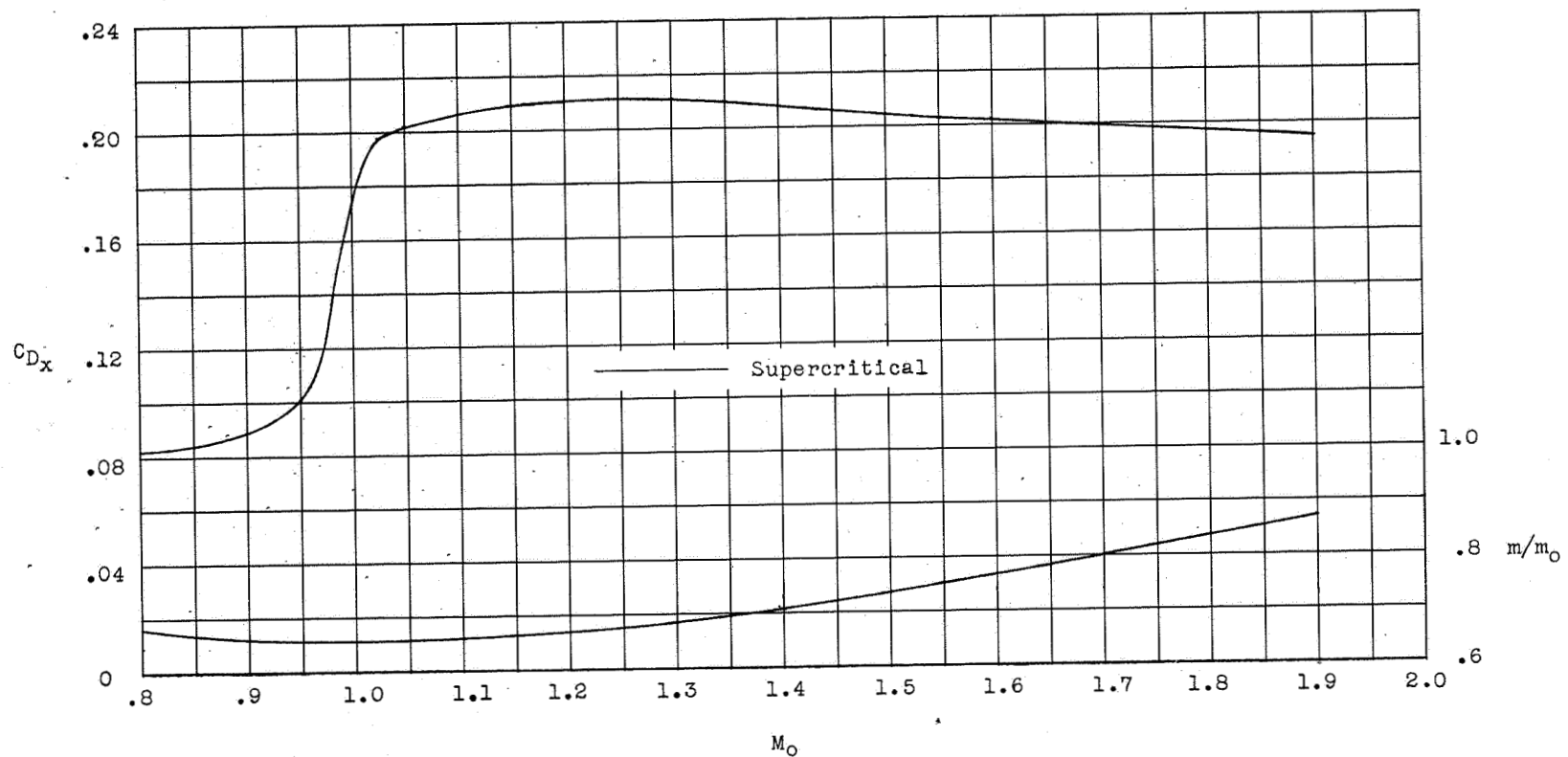
(i) 17-parabolic-39.

Figure 6.- Continued.
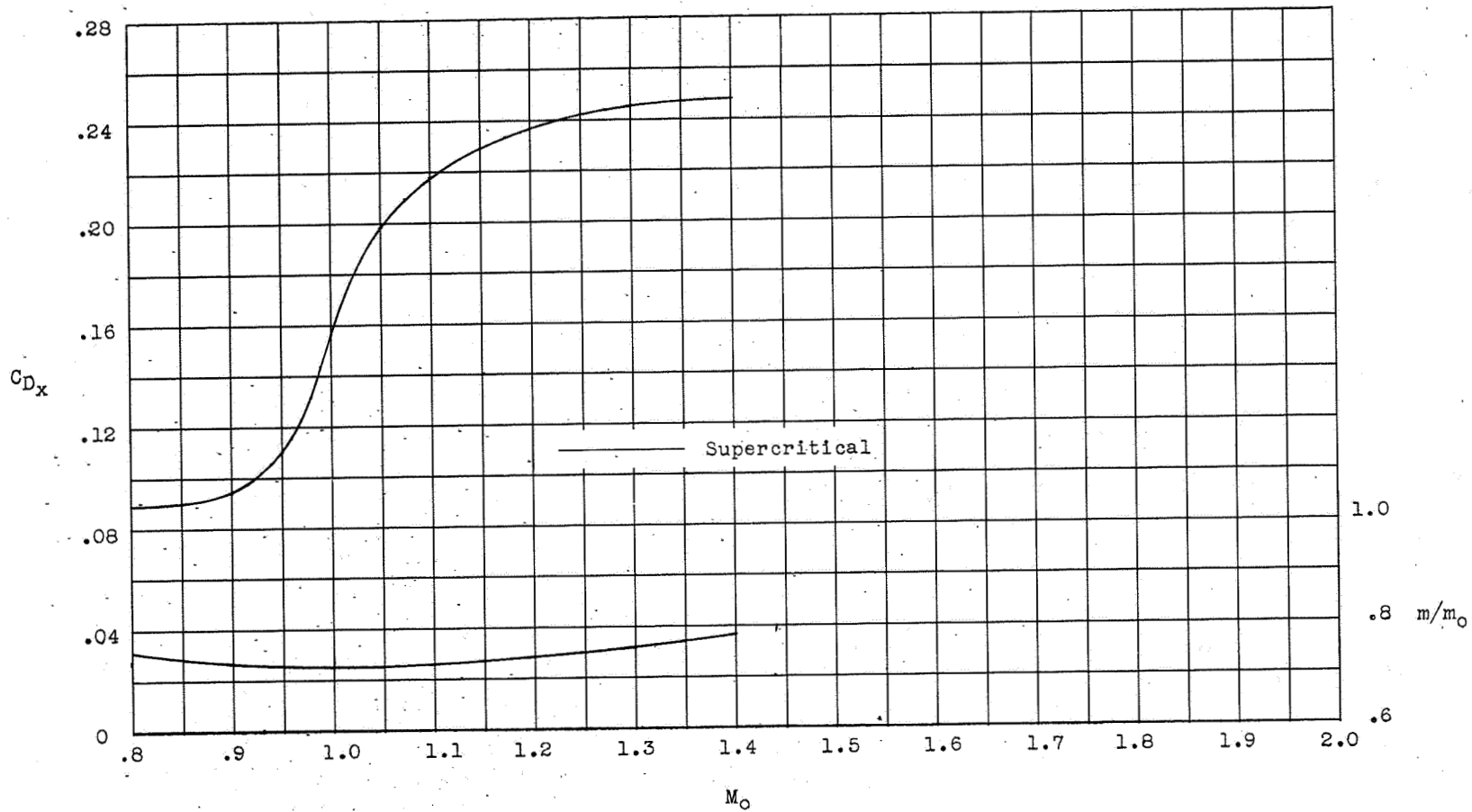
(j) 1-series.

Figure 6.- Concluded.
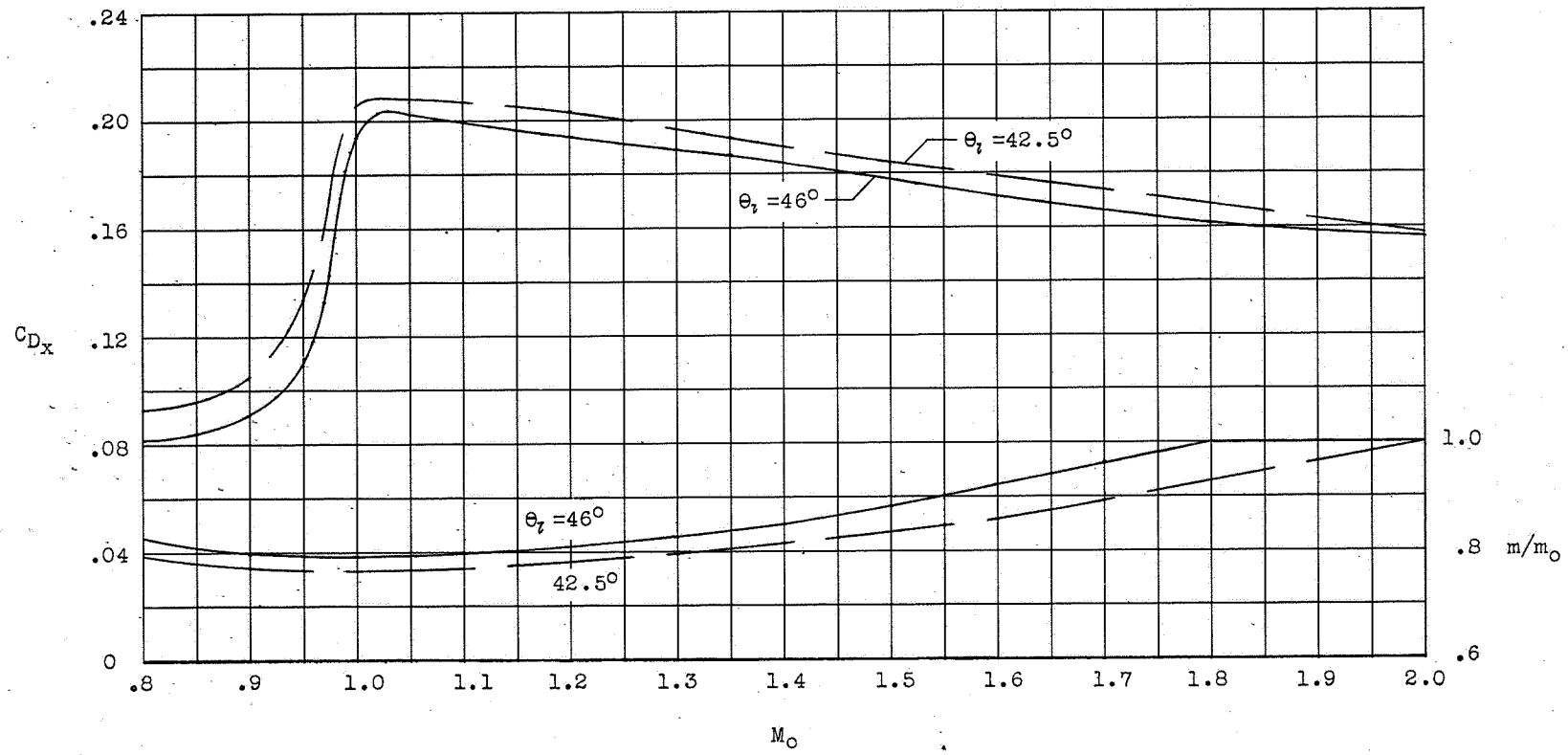
(a) 12-conic.

Figure 7.- Effect of axial cone position on external drag and mass-flow ratio at supercritical flow rates.
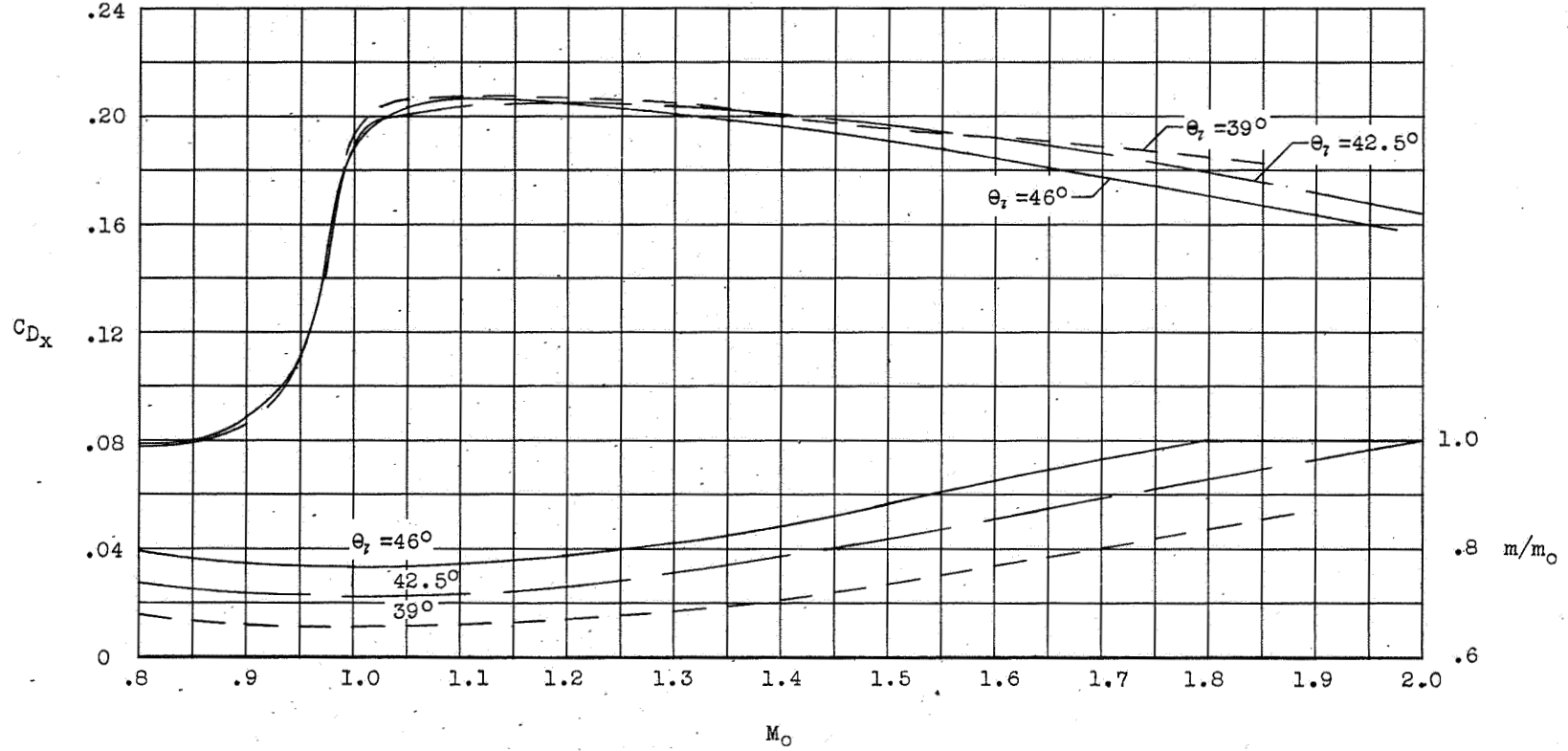
(b) 17-conic.

Figure 7.- Continued.
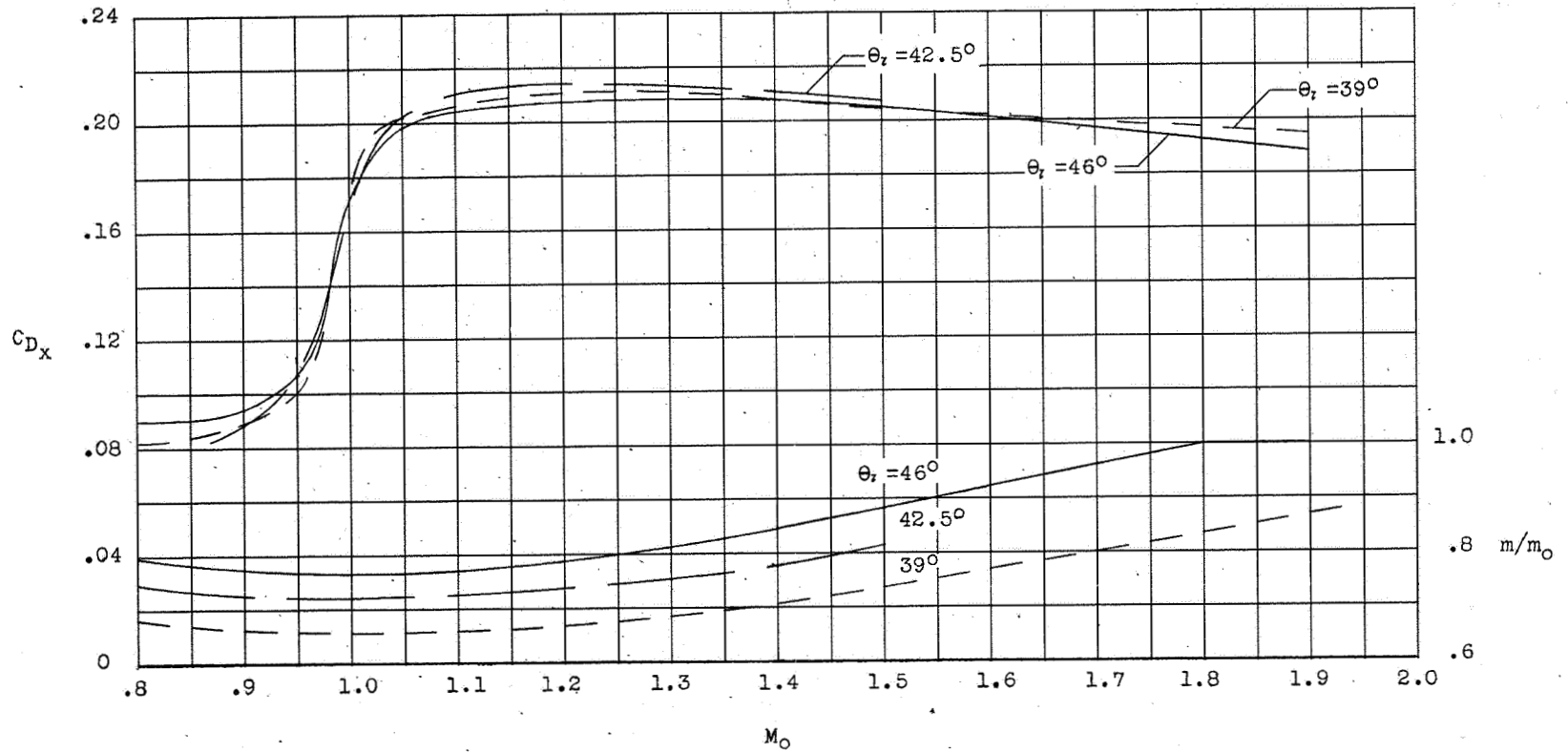
(c) 17-parabolic.

Figure 7.- Concluded.
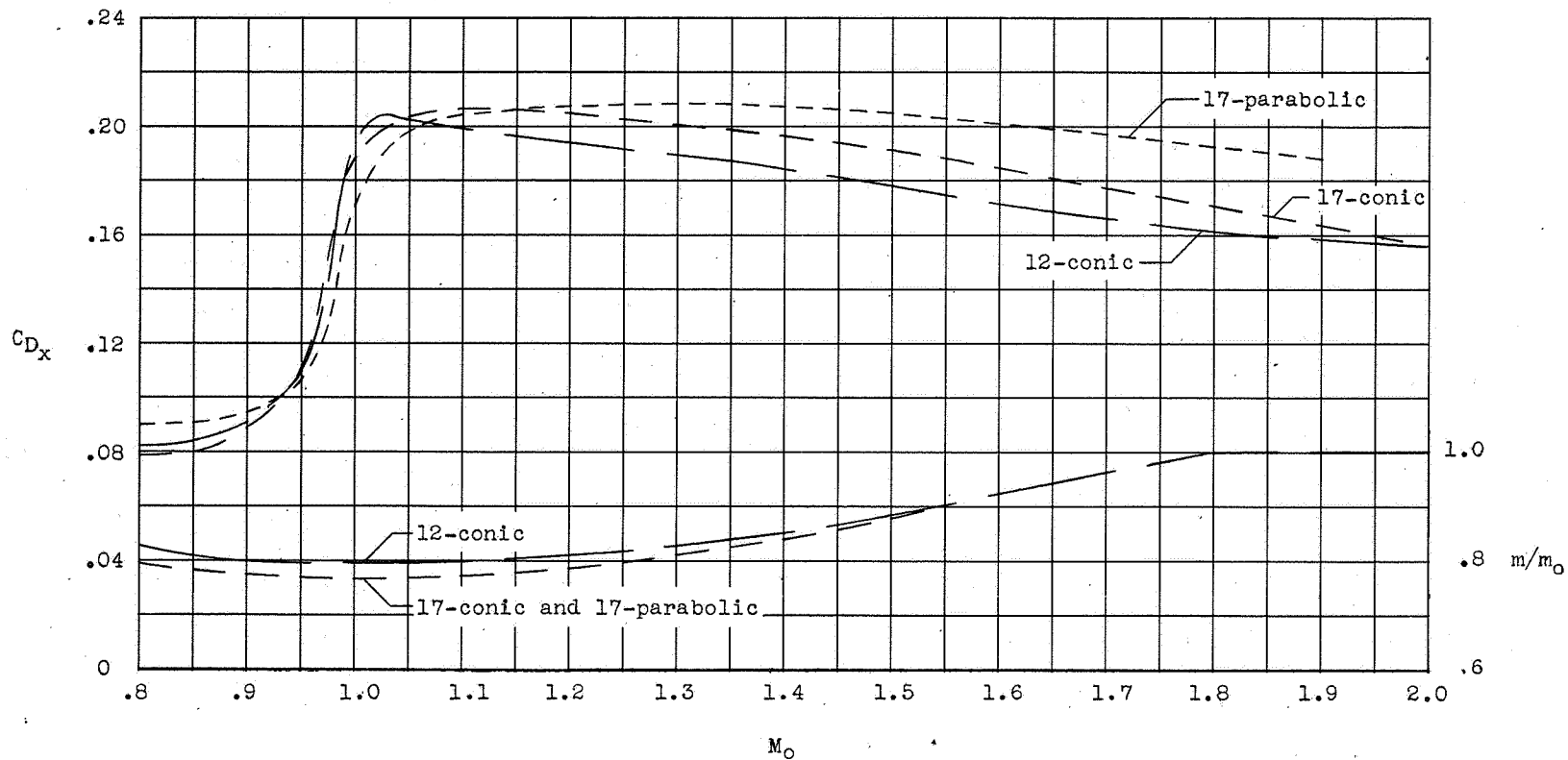
(a) $\theta_l = 46°$.

Figure 8.- Comparison of external drag coefficient at supercritical mass-
flow ratios as a function of Mach number for the various profiles.
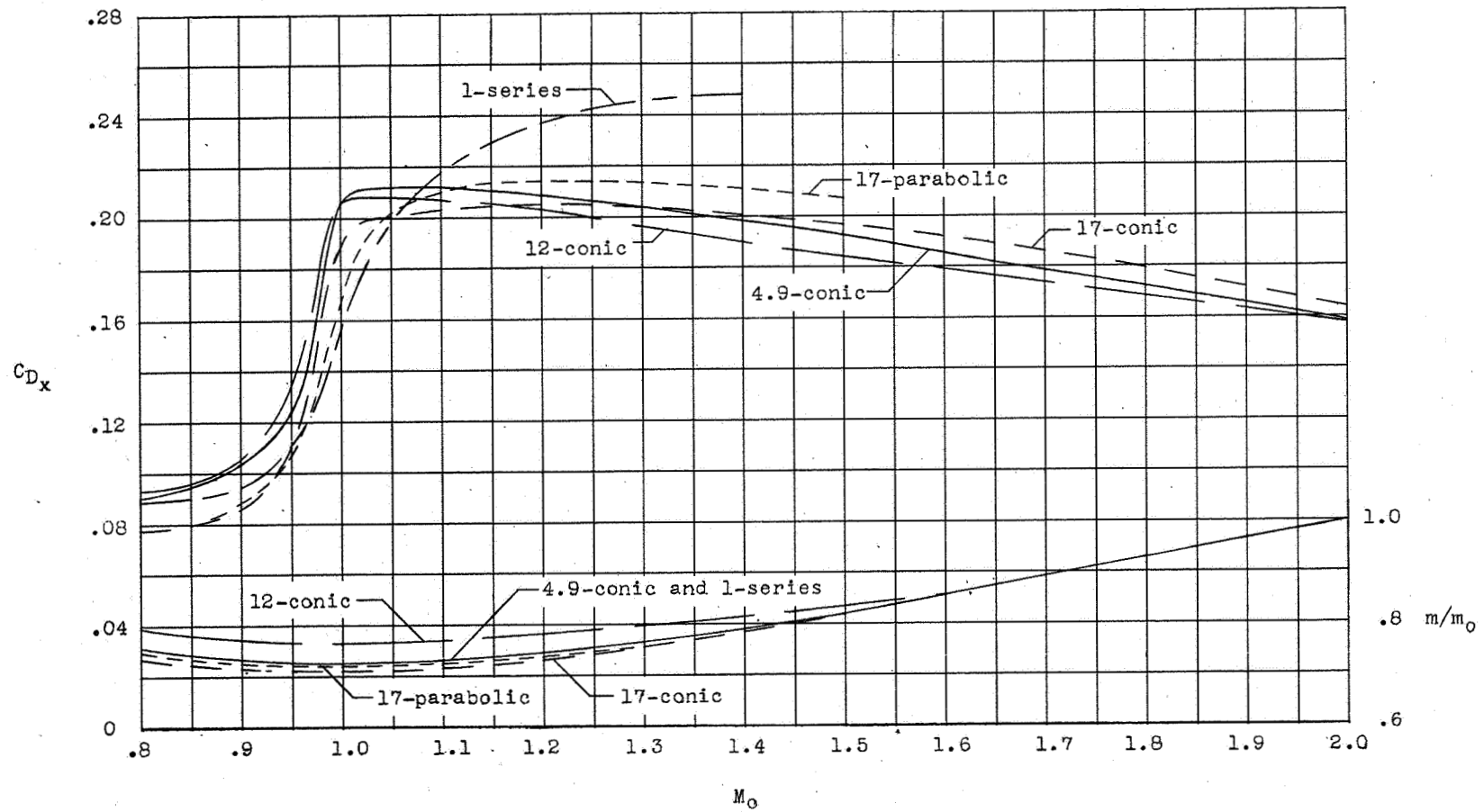
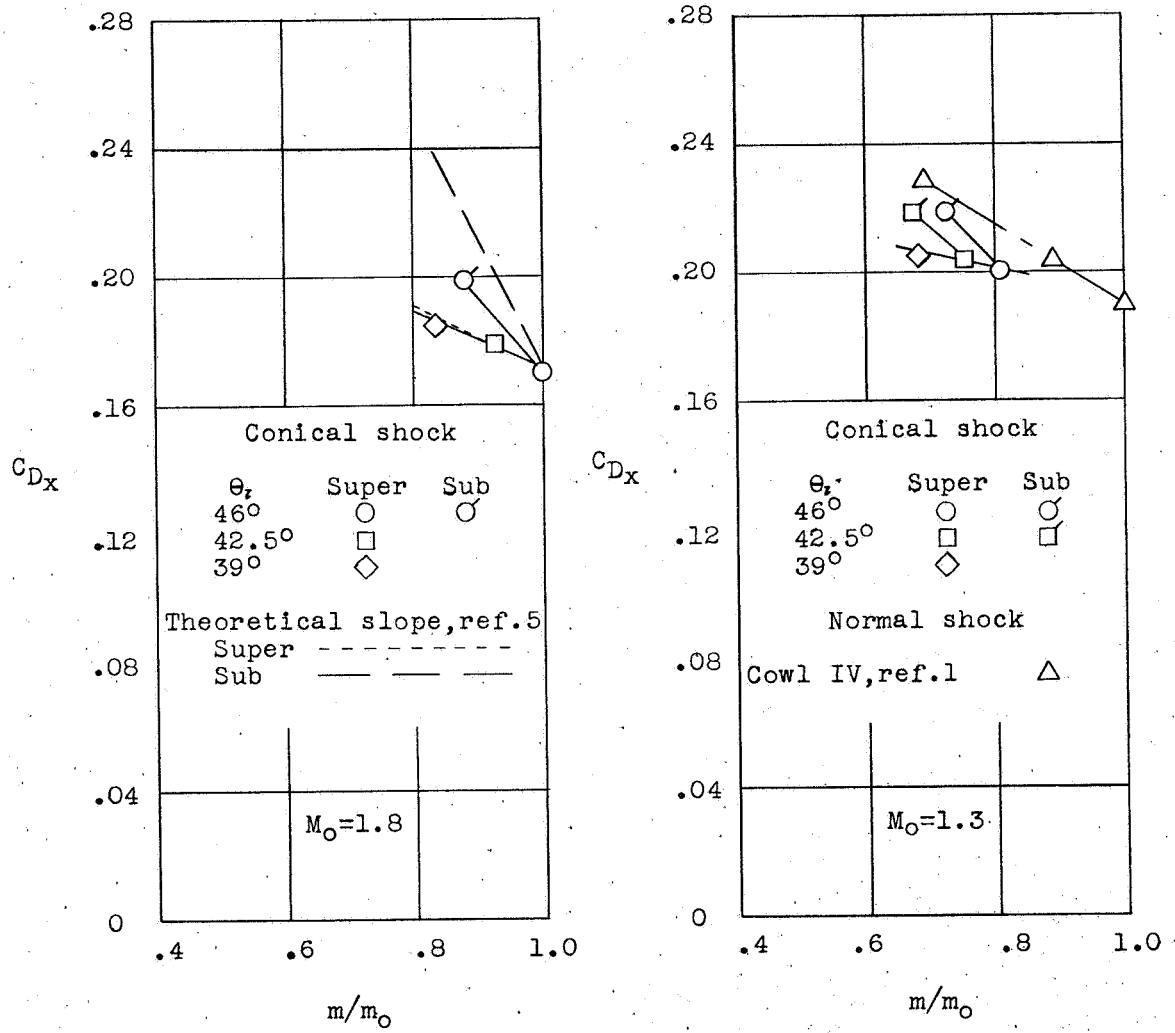(b) $\theta_l = 42.5^\circ$.

Figure 8.- Concluded.
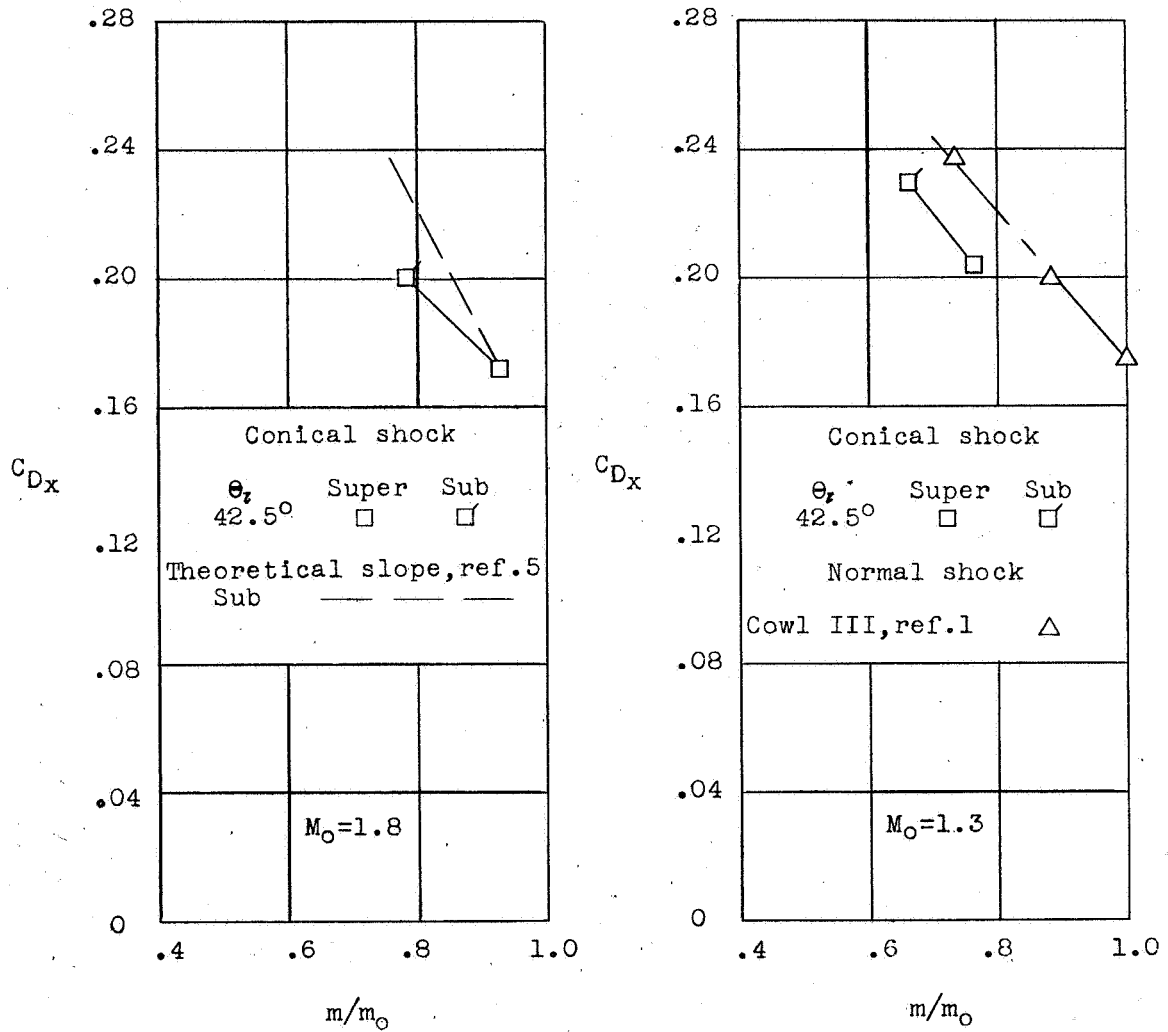
(a) 4.9-conic.

Figure 9.- Variation of external drag coefficient with mass-flow ratios
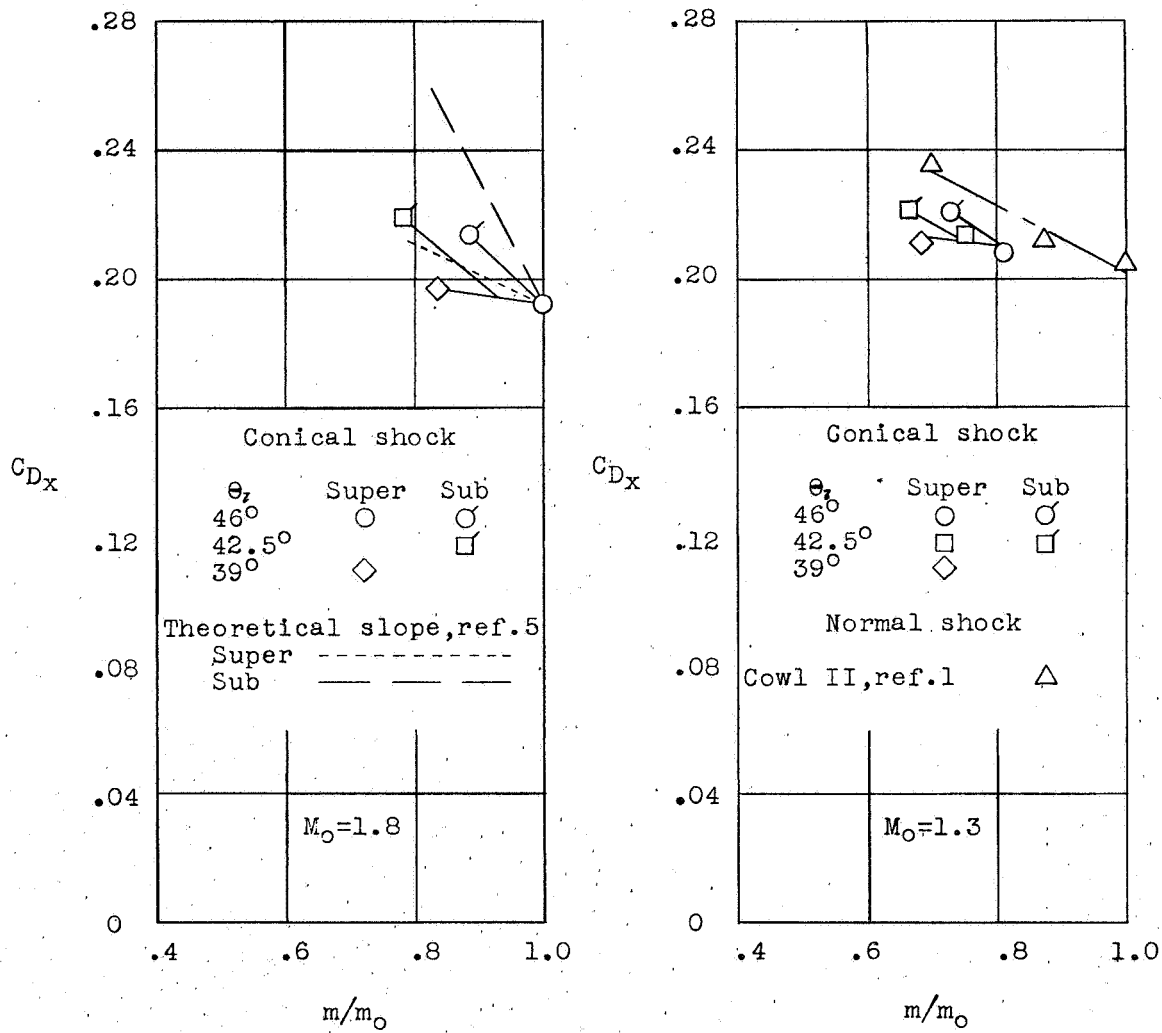for the various profiles.
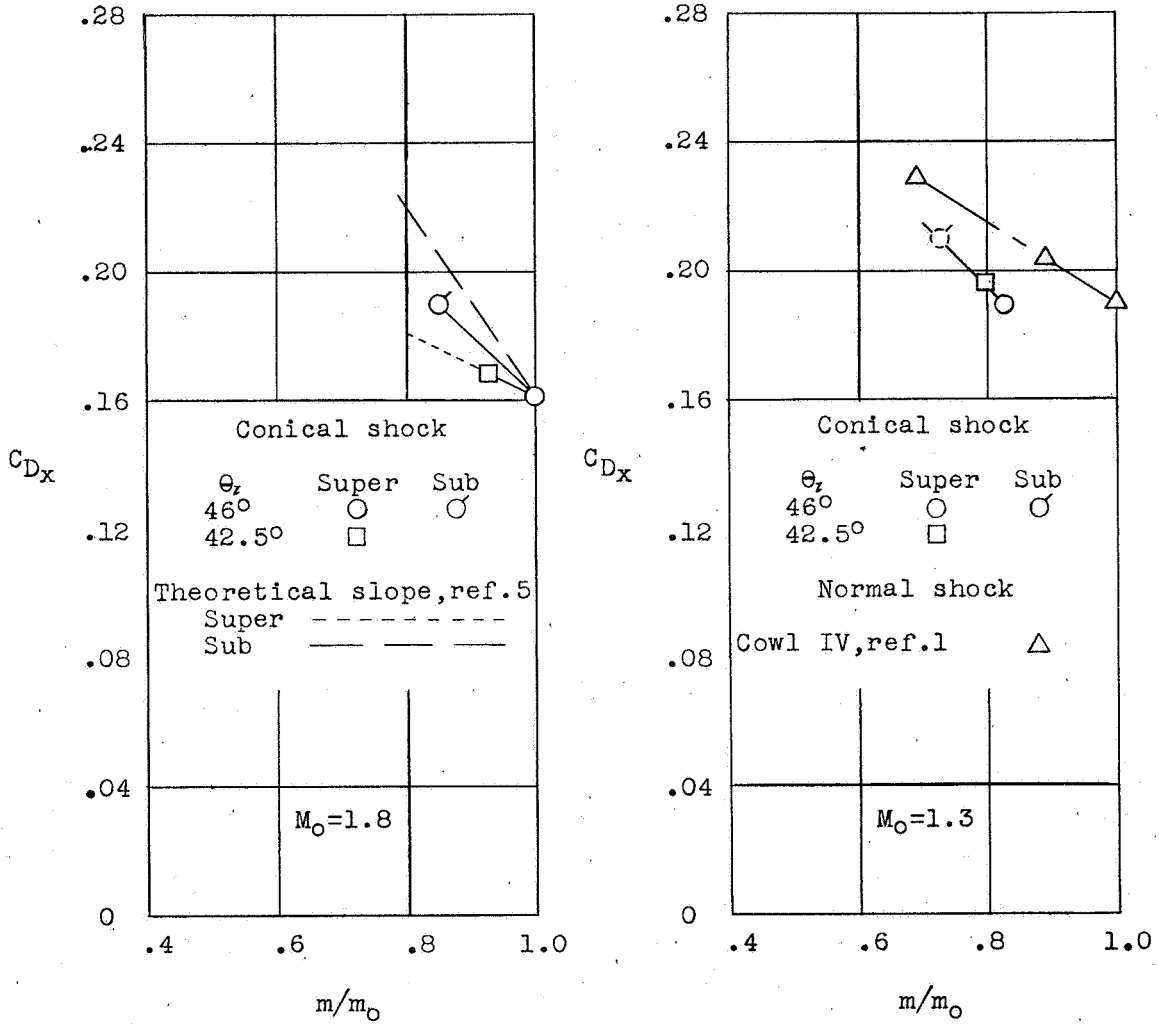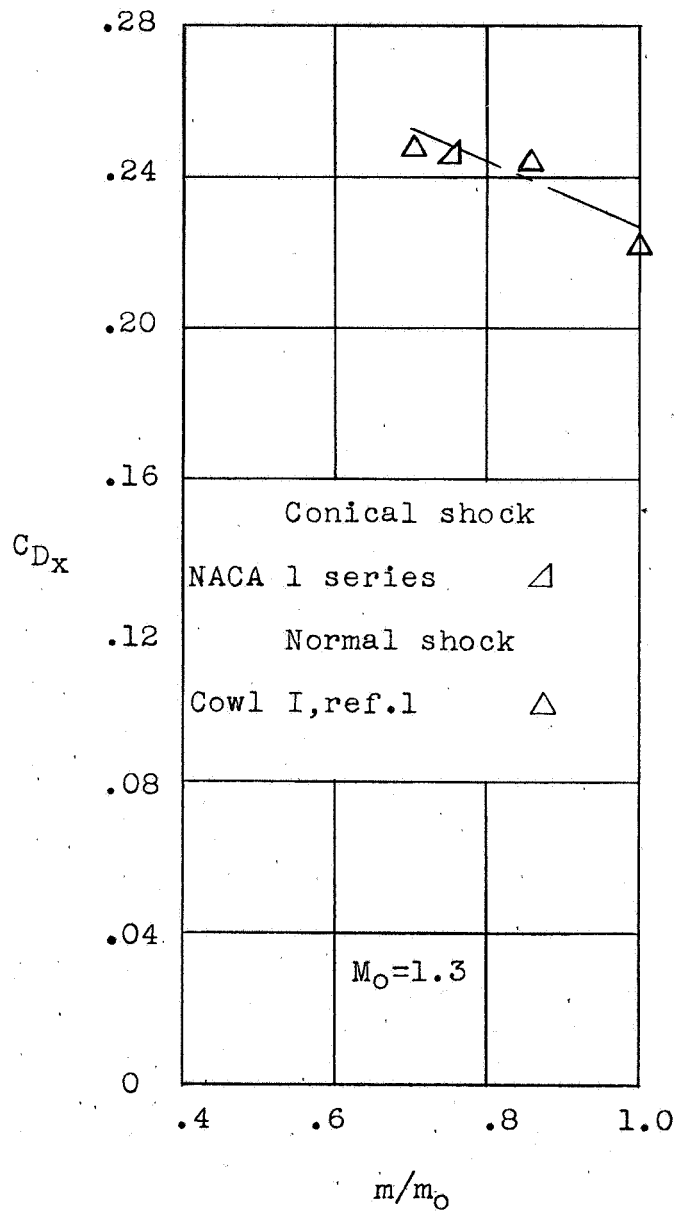
(b) 12-conic.

Figure 9.- Continued.

(c) 17-conic.

Figure 9.- Continued.

(d) 17-parabolic.

Figure 9.- Continued.

(e) 1-series.

Figure 9.- Concluded.